Miner Petrol (2012) 106:193–216
DOI 10.1007/s00710-012-0224-8

ORIGINAL PAPER

Multi-batch, incremental assembly of a dynamic magma chamber: the case of the Peninsula pluton granite (Cape Granite Suite, South Africa)

Federico Farina · Gary Stevens · Arnaud Villaros

Received: 10 December 2011 / Accepted: 13 July 2012 / Published online: 16 August 2012

Abstract The S-type Peninsula Pluton (South Africa) exhibits substantial compositional variability and hosts a large variety of mafic and felsic magmatic enclaves with contrasting textures and compositions. Moreover, the pluton is characterized by mechanical concentrations of K-feldspar megacrysts, cordierite and biotite, generating a complex array of magmatic structures including schlieren, pipes, and spectacular sheeted structures. Chemical evidence indicates that the pluton is constructed incrementally by rapid emplacement of numerous magma pulses. Field, and textural data suggest that magmatic structures form by local flow at the emplacement level of highly viscous crystal-rich magmas (i.e. crystallinity up to 50 vol.%) through magma mushes assembled from older batches. At the time of arrival of relatively late magma batches, some areas within the pluton had achieved crystal fractions that allowed the material to act as a solid, whilst maintaining enough melt to prevent formation of sharp intrusional contacts. Magmatic structures represent "snapshots" of processes that operate in multiphase crystal-rich mushes and their genesis is due to mechanical and thermal instabilities in the crystal-rich magma chamber that are triggered by the emplacement of pulses of new magma derived from the melting of a compositionally variable metasedimentary source.

Editorial handling: L. Danyushevsky

Electronic supplementary material The online version of this article (doi:10.1007/s00710-012-0224-8) contains supplementary material, which is available to authorized users.

F. Farina (✉) · G. Stevens
Department of Earth Sciences, University of Stellenbosch,
Private Bag X1,
7602 Matieland, South Africa
e-mail: fannak@gmail.com

G. Stevens
e-mail: gs@sun.ac.za

A. Villaros
Laboratoire Transfert Lithosphèrique, Université Jean Monnet,
23 rue Dr Michelon,
42000 Saint Etienne, France
e-mail: arnaudvillaros@gmail.com

Introduction

A growing body of field, geochronological and geochemical evidence (e.g. Glazner et al. 2004; Michel et al. 2008; Farina et al. 2010; Miller et al. 2011) suggests that granite (sensu lato) plutons are constructed incrementally by amalgamation of pulses of magma (i.e. magma batches) over periods of time ranging from tens of thousands (Michel et al. 2008) to millions of years (e.g. Coleman et al. 2004; Matzel et al. 2006). The emplacement of individual increments takes place at rates several orders of magnitude faster than the long-term average pluton growth rate (e.g. Villaros et al. 2009a) so that different parts of what have been mapped as single continuous bodies may differ in age. The volume of each new magma addition is likely to be small compared to the pluton, and thus the degree of crystallization may vary substantially within different portions of the pluton at any given time during its crystallization.

The paradigm shift from the customary view of plutons crystallizing from very large magma volumes emplaced in a single episode, to that of incremental growth through many discrete injections has a crucial influence on the way we conceive of granitic systems. The interplay between the volume and frequency of emplacement of magma batches influences the temperature-time paths of individual magma pulses, as well as the background temperature of the magma chamber, and thus controls both the potential for interaction between magma pulses over time and the capacity of the system to generate a large long-lived reservoir of mobile magma (e.g. Annen 2011). In addition, the multi-batch incremental model

has renewed the debate about the relative importance of different processes in shaping the chemical composition of granitic systems. In fact, for plutons constructed from small and fast-crystallizing magma pulses, processes active during and after emplacement (e.g. fractional crystallization) of individual batches are likely to be second-order processes that modify magma increments, whose bulk composition is mostly source-inherited (e.g. Clemens et al. 2009). Following this interpretation, chemical heterogeneities in granitic plutons are regarded as reflecting processes in the source that are transferred to the emplacement level by different magma batches that fail to mix efficiently during emplacement. Alternatively, as recently documented by Reichardt et al. (2010) and Hasalová et al. (2011) for leucosomes and leucogranitic dikes in the Karakoram Shear Zone (Ladakh, India) magma mixing may occur during magma segregation and transfer because magma batches, produced by melting of different sources, use the same pathways. In this case anatexis occurred through a water present process and may not be directly relevant to magma migration from the high temperature fluid absent sources that produce most of high level intrusions and eruptive systems. However, it does demonstrate that magma mixing may begin in the plumbing systems through which magmas ascend. In fact, ascent may be the period in a magmas evolution, where mixing is most readily accomplished.

The idea of plutons growing in-situ by amalgamation from many dike-fed increments has been questioned by authors describing a complex array of widespread magmatic structures that typically are interpreted to indicate accumulation of mafic minerals and large K-feldspar crystals with different magmatic histories (Weinberg et al. 2001; Wiebe et al. 2007; Žák and Klomínsky 2007; Paterson 2009). Magmatic structures (e.g. tubes, pipes, ladder dikes, plumes) are believed to be the result of local convection in crystal-rich magmas (i.e. crystals >50 vol.%) and have been regarded as frozen evidence of late-stage multiphase magma flow within large magma chambers (e.g. Paterson et al. 2005). According to Paterson (2009) the widespread occurrence of magmatic structures of this type in the Tuolumne Intrusive Suite (California, USA) is explainable by the existence of a laterally or vertically extensive magma chamber in which initially dispersed minerals are brought together, rather than a dike or sill construction model as previously suggested by Coleman et al. (2004) and Glazner et al. (2004). In addition, support for extensive mixing and mingling in the magmatic system is provided by mineral-scale studies that show evidence of complex crystal exchange between different magmas. In particular, elemental and isotopic data, along with petrographic and textural observations indicate that many crystals in volcanic and plutonic rocks have not crystallized from the magma (i.e. glass/groundmass) in which they are now hosted, but rather are inherited from magmas that existed at different places and times in the magma system (e.g. Davidson et al. 2007). These lines of evidence have been used to promote the view that magma chambers are sufficiently spatially and temporally extensive to permit active processes such as melt fractionation, segregation and interaction between resident and replenishing magmas.

The widespread apparent conflict between the idea of plutons formed incrementally by emplacement of numerous small magma pulses and that of extensive and compositionally zoned magma chambers within which magma flow occurs, might be more about what investigators choose to emphasis than about how plutons actually form. Contributions supporting the incremental assembly of granitic plutons generally emphasize how the magma batches cool below the solidus quickly and thus they exclude in-situ fractional crystallization and magma mixing as suitable processes to account for the chemical variations preserved in granitoids (e.g. Glazner et al. 2004). In these contributions magmatic structures may be overlooked or are not described or considered minor features. Alternatively, magmatic structures are interpreted as being formed by flow in dynamic magma chambers and thus they are considered evidence of magma movement at the emplacement site leading to both crystal mixing and fractional crystallization (e.g. Paterson 2009). However, those contributions focussing on the description and interpretation of magmatic structures do not commonly deal with the problem of the origin of chemical variability in granitic plutons (e.g. Wiebe et al. 2007).

The duration of pluton assembly; the size and frequency of magma additions to the pluton; the degree to which magma evolution takes place within the larger magma chamber or within sub-domains perhaps best represented by individual magma batches; the nature of the main processes controlling geochemical variations in individual pluton and granitoid suites; as well as the relationship between batholiths-sized bodies and large volume high-silica rhyolites (e.g. Bachmann and Bergantz 2008) remain key issues in understanding granitoid magma systems. The Peninsula pluton (Cape Granite Suite, South Africa) is characterised by a great deal of chemical variability that has been interpreted to reflect a source control on magma chemistry and multi-batch pluton assembly (Villaros et al. 2009a, b, 2012). However, the pluton is also characterised by abundant magmatic structures and magmatic enclaves that have never been described in detail and that would, following arguments of the type put forward by Paterson (2009), be interpreted to indicate the existence of a large, active magma chamber. Consequently, the Peninsula pluton represents an ideal place within which to explore the relationship between incremental pluton growth and the formation of magmatic structures.

The Peninsula pluton in context

The great elemental and isotopic variability exhibited by the S-type igneous bodies of the Cape Granite Suite has recently been the focus of numerous studies (Stevens et al. 2007; Villaros et al. 2009a, b; Harris and Vogeli 2010; Villaros et al. 2012). Most of these studies were intended to identify a general model for the petrogenesis of S-type granites. In fact, although it is well established that S-type granite magmas form by fluid-absent partial melting of aluminous clastic sediments (i.e. metapelites and metagreywackes) and the nature of the melting reactions involved is well known by theoretical and experimental studies (e.g. Vielzeuf and Montel 1994) as well as by the study of migmatites (e.g. Sawyer 1996), many different processes have been proposed to account for the substantial geochemical range exhibited by granites, with bulk rock wt% SiO_2 commonly ranging from approximately 65 to 78. Recently, Clemens and Stevens (2012) have reviewed the different mechanisms that have been suggested to be responsible for the production of heterogeneity in granitic magmas. The most commonly invoked processes are restite unmixing, fractional crystallization, mixing with mantle-derived magmas and wall-rock assimilation.

Using major and trace element data from the Cape Granite Suite Stevens et al (2007) and Villaros et al. (2009a, b) suggested that the chemical variability typically exhibited by S-type suites and individual bodies is inherited from the source by three different mechanisms: (i) Source control of the melt composition. Within the granites this is reflected in variation in the concentration of elements that are compatible within the melt (e.g. K_2O, Sr, Ba, Na etc) and this reflects the composition and proportions of the reactant minerals that melted in the source. These elements show substantial compositional variation at any given bulk rock MgO + FeO^T value. (ii) Peritectic assemblage entrainment control on magma composition. Elements that are concentrated within the reactant minerals at concentrations higher than can be accommodated within the melt are expressed as the peritectic assemblage produced by the breakdown of hydrous phases. Stevens et al. (2007) proposed that the strong positive correlation between Ti and Mg + Fe inherent to all S-type granites is produced as a consequence of entrainment of the garnet- and ilmenite-bearing peritectic assemblage into the magma in proportions that range from 0 to approximately 30 mol%. (iii) Co-entrainment of the accessory mineral suite as a control on trace element composition. Accessory minerals, commonly hosted within biotite in the source, are co-entrained with the peritectic assemblage because of their small crystal size and availability at the sites of melting. Consequently, trace elements concentrated within these minerals (Hf, Zr, REE) correlate positively with major elements that reflect peritectic assemblage entrainment.

The Peninsula pluton is characterised by complex magmatic structures occupying a volumetrically significant part of the intrusion and it also contains numerous magmatic enclaves displaying variable texture, size and composition. Magmatic structures and enclaves may provide important constraints on the relative contribution of various petrogenetic processes playing a role in shaping the chemical composition of the magma system. Despite this, these features of the Peninsula pluton have yet to be studied in detail. This work seeks to document these features and analyse the processes that have formed them. In doing so, it is anticipated that a deeper understanding will emerge of the interplay between multiple magma batch injection into magma chambers and the origin of magmatic structures.

Geological background

The Peninsula pluton is one of the igneous bodies forming the Cape Granite Suite. The Suite outcrops over a distance of more than 500 km along the Southern and Western Cape coast and is mainly composed of S- and I-type granitic bodies formed between 556 and 520 Ma (Scheepers and Armstrong 2002), but also includes rare and younger A-type granites, gabbros, diorites and ignimbrites (≈520–510 Ma; Joordan et al. 1995; Scheepers and Poujol 2002). The plutons intrude shales, greywackes, conglomerates, limestones and mafic metavolcanic rocks of the Malmesbury Group, which represent a 950 to 610 Ma volcano-sedimentary succession (e.g. Gresse and Scheepers 1993; Scheepers 1995) formed as an accretionary mélange during Gondwanan convergence of Kalahari and Rio de la Plata cratons and the closure of the Adamastor Ocean (Fig. 1a; Rozendaal et al. 1999). The rocks of Malmesbury Group are metamorphosed up to lower greenschist facies grades (Rozendaal et al. 1999; Belcher and Kisters 2003).

The S-type granites of the Cape Granite Suite formed between 556 and 534 Ma (U-Pb zircon and monazite ages; Scheepers and Armstrong 2002; Villaros et al. 2011) and are slightly older than I-type granites emplaced between 540 and 520 (U-Pb zircons; Da Silva et al. 2000). The source of the S-type plutons is considered to be a higher grade equivalent of the Malmesbury Group rocks (e.g. Harris et al. 1997). In fact, these metasedimentary rocks have $\delta^{18}O$ values that are consistent with them being appropriate source materials for the production of S-type granites such as the Peninsula pluton (Harris and Vogeli 2010). The Cape Granite Suite consists of four major S-type plutons (Darling, Saldanha, Stellenbosch and Peninsula) located south of the NW-SE trending Colenso Shear Zone and showing similar compositional variation from leucogranite to granodiorite (Stevens et al. 2007). The S-type granites typically contain cordierite, biotite, muscovite, plagioclase, quartz, and large

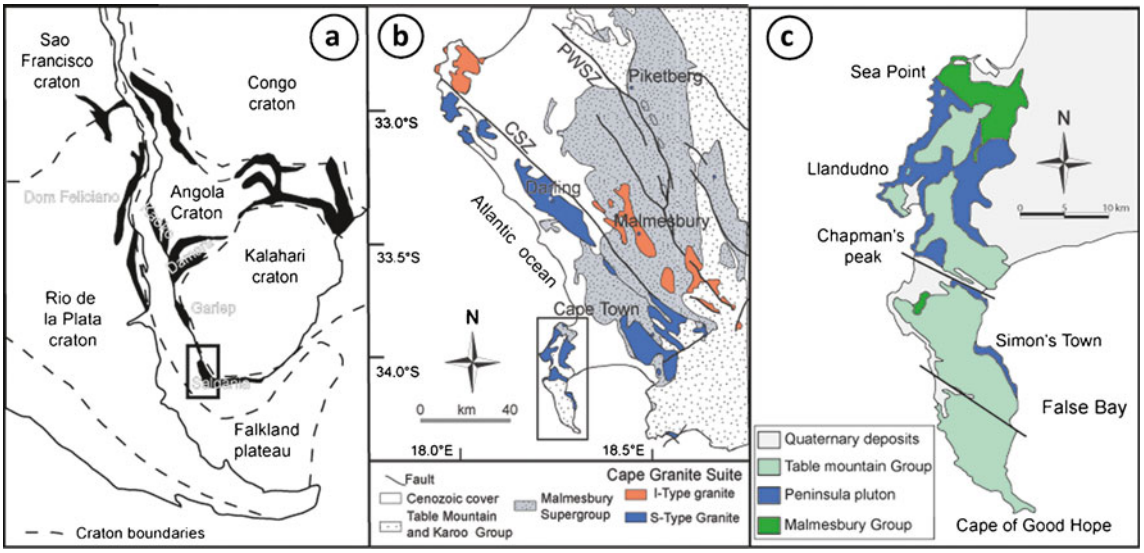

Fig. 1 **a** Paleogeographic reconstruction of the Saldania orogen at 550 Ma; **b** Geological map of the Cape Granite Suite; CSZ stands for Colenzo Shear Zone, PWSZ for Piketberg-Wellington Shear Zone; **c** Geological map of the Peninsula pluton. Figure modified after Villaros et al. (2009a, b)

K-feldspar phenocrysts with garnet preserved in some rocks (Villaros et al. 2009b). Garnet is typically partially replaced by cordierite and biotite (Villaros et al. 2009b).

The Peninsula pluton is the southernmost body among the S-type granites of the suite and crops out along the Cape Peninsula, a thin finger of land stretching southward from Cape Town to Cape Point (Fig. 1b, c). The Peninsula pluton is essentially undeformed and is characterized by little alteration, apart from common pinitisation of cordierite, and contains rocks that record almost the full range of compositional variability exhibited by the S-type granites of the Cape Granite Suite. The contact between granite of the Peninsula pluton and the metasedimentary rocks of the Malmesbury Group is best exposed in a spectacular outcrop at Sea Point (Figs. 1c and 2a) that was first described by Charles Darwin during his voyage of scientific discovery on H.M.S. Beagle in 1837 (Darwin 1844). This is one of a very few areas where the granite is deformed over a narrow zone along the contact. The pluton is unconformably overlain by the Ordovician quartzite of the Table Mountain Group (Fig. 2b). In-situ zircon U-Pb ages from the monzogranite gives crystallization ages of 540±5 Ma (Scheepers and Armstrong 2002; Villaros et al. 2011).

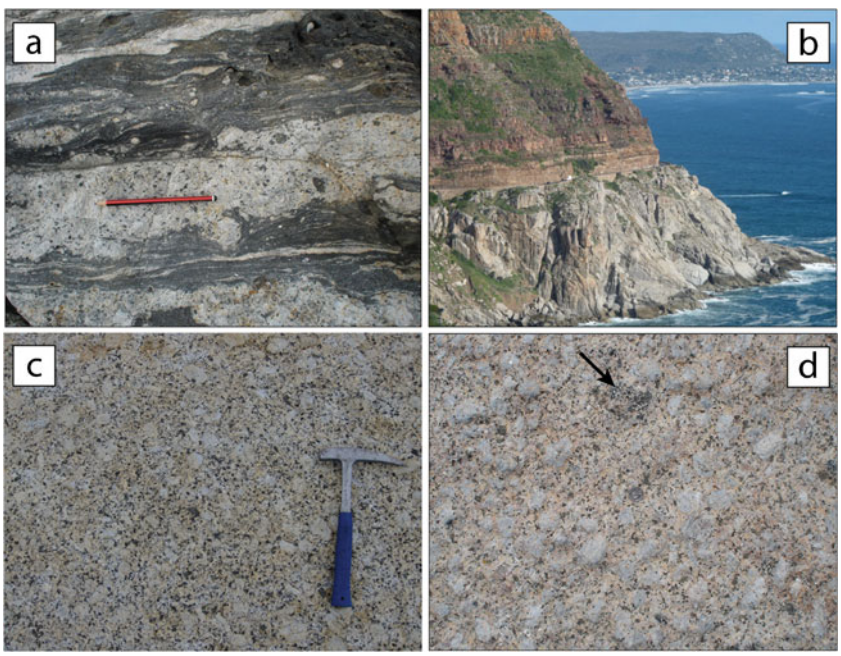

Fig. 2 Field photographs of Peninsula monzogranite. **a** Contact between the monzogranite and metasedimentary rocks of the Malmesbury Group; this is the outcrop described by Darwin in 1844. **b** Panoramic view of the Chapman's Peak roadway constructed along the unconformity between granite and the overlying Table Mountain Group. **c** Granite area rich in cordierite and biotite. The hammer is 32 cm in length. **d** Typical field appearance of the K-feldspar megacrystic monzogranite, the *black arrow* indicates a large quartz-tourmaline clot in a megacryst-free domain. The coin is 2 cm in diameter

Analytical methods

Whole-rock geochemistry

Due to the relatively poor exposure of fresh granite inland, the majority of the samples in this study were collected along the coast. Samples of approximately 8 kg were collected and between 4 and 6 kg of material was crushed and analyzed for major and trace elements at the Central Analytical Facility, University of Stellenbosch, South Africa. Nd separation was performed at the Department of Geological Sciences, University of Cape Town, isotope analyses were performed at the Africa Earth Observatory Network (AEON), Cape Town, South Africa.

Loss on ignition was calculated by placing powdered samples in an oven at 1,000°C for 1 h. Major element compositions were analyzed by X-ray fluorescence spectrometry (XRF) on glass beads prepared with La-free flux. Internal standards were basalt BHVO-1 and granite NIM-G. For the granite, calculated uncertainties (twice the measured deviations for the granite standard expressed in wt%) are: 0.35 for SiO_2, 0.02 for TiO_2, 0.12 for Al_2O_3, 0.15 for FeO^T, 0.01 for MnO, 0.02 for MgO, 0.07 for CaO, 0.10 for Na_2O, 0.02 for K_2O and 0.01 for P_2O_5. Results are plotted after normalization to 100 wt.% volatile-free. Trace element compositions have been obtained from the same fused beads used for major element determination by applying the method described by Eggins (2003) and analysed using an Agilent 7500ce ICP-MS coupled with a Nd-YAG 223 nm New Wave LASER ablation (LA) system operating at a 12 Hz frequency with a mixed He-Ar carrier gas. Three analyses (each comprising a 30 s blank followed by data collection for 60 s) on each whole rock fused disc were obtained using a 100 μm diameter aperture, and the results averaged. After every three samples (i.e. every 10th analysis) NIST612 (Pearce et al. 1997) glass bead was analysed as a calibration standard, in addition to fused discs of NIM-G (granite) and BHVO-1 (basalt) that were analysed as secondary standards. Data were collected in time-resolved mode and were reduced using the SiO_2 content measured by XRF as the internal standard. For each element, the reproducibility of replicate analyses of the samples, and deviation from the certified values of the secondary standards are less than 10 %, and mostly less than 5 % relative.

Neodymium chemical separation followed the procedure described in detail by Míková and Denková (2007). The Nd isotopic data were obtained with a Nu Instruments NuPlasma HR ICP-MS coupled to a DSN-100 desolvating nebuliser. Data are reported relative to the accepted value of $^{143}Nd/^{144}Nd = 0.512115$ for the JNdi-1 standard (Tanaka et al. 2000). Analyses of the international standard BHVO-2 yield a $^{143}Nd/^{144}Nd$ value of 0.513000±0.000012 (±2sd). These data compares well with published values for BHVO-2, e.g. $^{143}Nd/^{144}Nd = 0.512984±0.000011$ (Weis et al. 2006). All Nd isotope data were corrected for Sm and Ce interference using the measured signal for ^{147}Sm and ^{140}Ce and natural Sm and Ce isotope abundances. Instrumental mass bias was corrected by normalizing to $^{146}Nd/^{144}Nd$ value of 0.7219, using the exponential law. Measured $^{143}Nd/^{144}Nd$ values are calculated to 540 Ma. Concentrations for Sm and Nd were measured on fused beads. The error for ε_{Nd} (t) is calculated considering an uncertainty of 4 % on the Sm and Nd concentrations and an error of ±4 Ma on the age of the pluton.

Mineral chemistry

The major element compositions of the rock-forming minerals in selected samples were analysed using a Leo® 1430VP Scanning Electron Microscope at the Department of Earth Sciences, Stellenbosch University, South Africa. Mineral compositions were quantified by EDX (Energy Dispersive X-ray) analysis using an Oxford Instruments 133 keV ED X-ray detector and Oxford INCA software. Beam conditions during the quantitative analyses were 20 kV accelerating voltage and 1.5 nA probe current, with a working distance of 13 mm and a specimen beam current of −4.0 nA. X-ray counts were typically ~7,000 cps, and the counting time was 50 s live-time. Analyses were quantified using natural mineral standards, and mineral chemical compositions were recalculated to mineral stoichiometries to obtain resultant mineral structural formulae. Comparisons between measured and accepted compositions of control standards within this laboratory, as a reflection of the accuracy of the analytical technique, have been published by Moyen et al. (2006).

Field relations and petrography

The Peninsula pluton

The Peninsula pluton is a coarse-grained monzogranitic intrusion that consists mainly of plagioclase (25–30 %), quartz (30–40 %), alkali-feldspar (15–25 %), biotite (<10 %), strongly pinitised cordierite (5–10 %) and minor garnet (Figs. 2 and 3). The accessory mineral assemblage is dominated by apatite and zircon, followed in abundance by monazite and ilmenite. Rounded clots of tourmaline and quartz reaching up to 10 cm in diameter occur locally (Fig. 2d) and rare crystals of allanite and fluorite have also been observed. The pluton is characterized by the occurrence of (5–15 vol.%) euhedral and inclusion-rich alkali feldspar crystals reaching up to 20 cm in length as well as by up to 30 mm diameter pseudomorphs of cordierite after garnet (Figs. 3 and 4c; Villaros et al. 2009b). Relict garnets

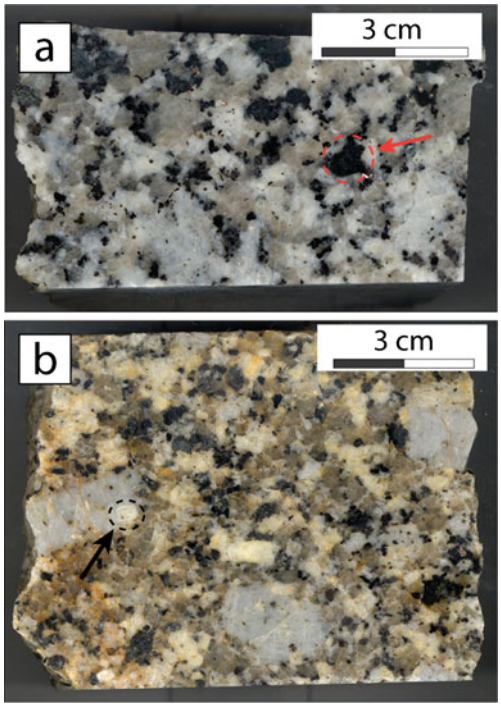

Fig. 3 Polished slab appearance of the monzogranite. **a** Quartz crystals are >1 cm in diameter, pinite pseudomorphs after cordierite reach up to 1 cm. The *arrow* indicates a pseudomorphosed cordierite crystal. **b** Plagioclase/alkali-feldspar proportion in the rock can be estimated due to the distinguishable yellowish colour of weathered plagioclase. The *arrow* indicates a large plagioclase crystal hosted in K-feldspar megacryst

are rounded to subhedral, free of inclusions and commonly cracked, with the fractures filled by plagioclase, K-feldspar and biotite. Cordierite crystals are completely replaced by aggregates of green-brown Ti-poor biotite and white mica as well as by very fine-grained mats of phyllosilicates varying under the polar microscope from grey to the typical third order blue of muscovite (Fig. 4a). The occurrence of K-rich phyllosilicates replacing former cordierite indicates that pinitisation has involved ingress of K^+-rich fluids.

Alkali feldspars can be divided into two separate populations. The first consists of euhedral crystals typically >2 cm in length (hereafter megacrysts) mostly characterized by a {010} tabular habit elongated on the c-axis. The megacrysts have Carlsbad twins, are commonly exsolved to perthite and host numerous inclusions of biotite, plagioclase, quartz and rarely cordierite. Mineral inclusions have smaller size relative to crystals in the host granite and tend to be more abundant at megacryst rims. The second alkali feldspar population consists of subhedral-anhedral perthitic crystals that are dominantly interstitial. Plagioclase crystals are euhedral, reach up to 1 cm in length and exhibit concentric normal zoning characterized by homogeneous cores (An_{30-35}) surrounded by an Ab-rich zone (An_{20-28}) and a thin albitic mantle (20–80 μm).

Biotite is the most abundant ferromagnesian mineral and forms individual crystals up to 5 mm in length that host inclusions of zircon, apatite, monazite and minor ilmenite.

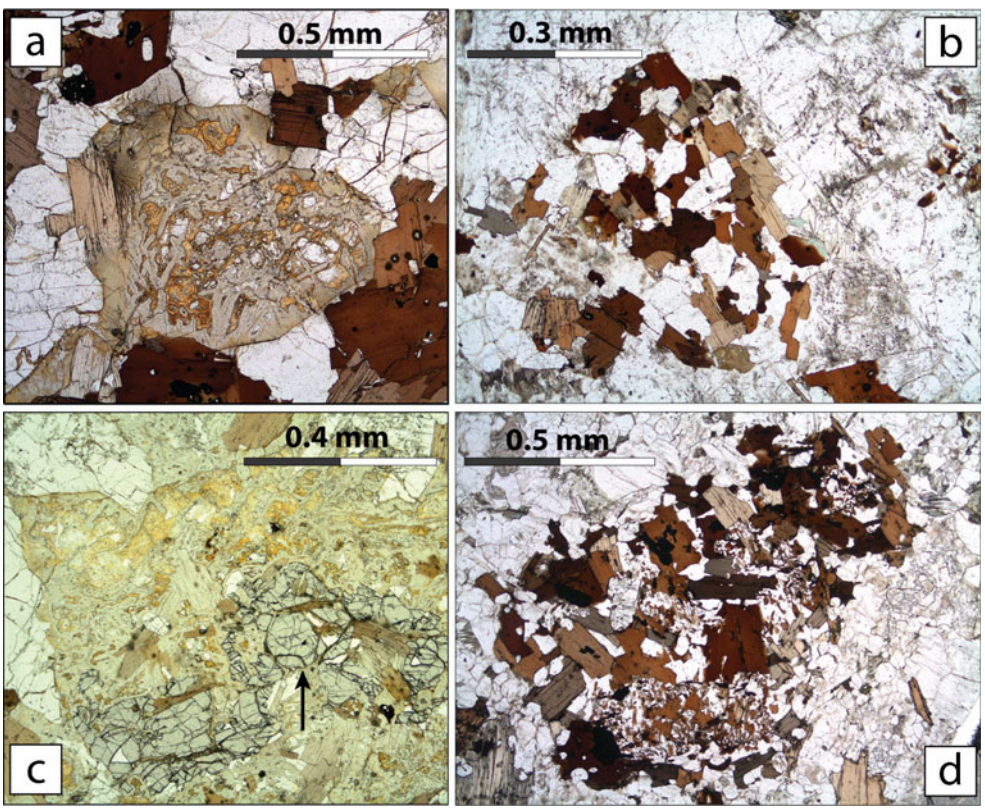

Fig. 4 Photomicrographs of typical rock textures. **a** Cordierite pseudomorph completely replaced by pinite. **b** Quartz-biotite clot with biotite mainly forming clot's rim. Quartz and biotite crystals are euhedral-subehedral and have similar sizes. **c** Large pinitized cordierite pseudomorph after garnet. The *arrow* indicates remnants of former inclusion-free garnet showing the characteristic high relief. **d** Quartz-biotite clot containing symplectic intergrowth of biotite and quartz

Fine-grained, inclusion-poor elongated biotite crystals are associated with muscovite in the replacement of cordierite and, in addition, biotite is often associated with quartz to form clots of up to 1 cm in diameter (Fig. 4b, d). These clots are widespread throughout the pluton and their size and abundance increase in the more mafic variety of the granite. In the clots, biotite and quartz crystals are finer-grained relative to those in the granite and biotite hosts many large ilmenite inclusions (up to 400 μm) so that, in some cases, ilmenite is by far the most abundant inclusion. Two different end-member textures have been recognized for the clots, in both of them the rim of the clot consists of biotite crystals that enclose quartz and biotite. In the first type, the core of the clot consists of euhedral to subhedral biotite and quartz crystals of a size similar to that of the biotite crystals forming the rim. In the second textural end-member the two phases form symplectic intergrowths (Fig. 4d). This second texture is characteristic of the more mafic granite types as well as of some enclaves and dikes. Biotite-quartz clots are interpreted to represent replacement of former orthopyroxene that is never preserved. This interpretation is supported by experimental studies on S-type granites predicting stability of orthopyroxene at high temperatures (Clemens and Wall 1981) and by textural evidence from other, compositionally similar bodies. In fact, similar biotite-quartz clots have been described by Maas et al. (1997) and Clemens and Benn (2010) for two Australian S-type granites; the Deddick and Mt. Disappointment plutons. Within these clots, remnants of former pyroxene are preserved (orthopyroxene for the Deddick pluton, clino- and orthopyroxene in the Mt. Disappointment). Moreover, orthopyroxene crystals occur in strongly peraluminous volcanic rocks of central Victoria (Australia) where the replacement reaction was halted by eruption (Clemens and Wall 1984).

Finally, it is worth noting that at outcrop scale, the monzogranite occasionally shows a magmatic fabric defined by the alignment of K-feldspar megacrysts. However, sporadic fabric development and rapid change in fabric orientation within individual outcrops, prevents the definition of a magmatic anisotropy at pluton-scale.

Magmatic enclaves, leucogranitic dikes and metamorphic xenoliths

The Peninsula pluton hosts a great variety of magmatic enclaves that have been subdivided according to their field appearance, mineralogy and chemical composition. The more representative enclave types, listed in order of abundance are: i) leucogranitic enclaves, ii) megacryst-free enclaves, iii) porphyritic granodiorite enclaves, iv) microgranitoid enclaves and v) coarse-grained mafic enclaves. These enclave types make up less than 1 vol.% of the pluton.

Leucogranitic enclaves are characterised by a rounded shape with diameter ranging from 10 to 50 cm. A few large elongated enclaves, reaching up to 5 m in length, have been also observed (Fig. 5). These rocks are fine- to medium-grained, with grain size positively correlated with enclave dimension: large enclaves are typically coarser-grained than small ones. Rock-forming phases are K-feldspar, quartz, plagioclase and minor biotite (<5 vol.%). Biotite is the only ferromagnesian phase and generally occurs as inclusion-poor crystals (<2 mm), sometimes forming clusters. Accessory phases are apatite, zircon and monazite. Tourmaline clots are also common. In some cases K-feldspar megacrysts and cordierite crystals in the granitic host accumulate at the enclave boundaries suggesting that during magma flow the leucogranitic enclaves were sufficiently crystallized to behave as solid objects.

Megacryst-free enclaves are equigranular, medium-grained, rounded to elongated domains presenting transitional to sharp contact with the host (Fig. 6a). Their margins are commonly slightly crenulated and alkali feldspar megacrysts from the hosting granite may occasionally straddle the enclave-host boundary or more rarely be fully incorporated as xenocrysts. Megacryst-free enclaves are commonly less than 0.5 m^2 in area. Rock-forming phases are quartz, plagioclase, alkali feldspar and biotite and muscovite clots probably replacing former cordierite.

Porphyritic granodiorite enclaves consist of phenocrysts of plagioclase, cordierite, quartz and biotite that are similar in size, habit and composition to the same minerals in the monzogranite and that are set in a fine- to medium-grained groundmass. K-feldspar megacrysts form up to 10 vol.% of the enclaves, are slightly to substantially smaller than those in the host granite and show xenomorphic resorption surfaces marked by an increase in the abundance of mineral inclusions. Garnet that has been partly replaced by cordierite

Fig. 5 Field photograph of a large leucogranitic enclave having angular shape. Megacrysts and microgranular enclaves are accumulated on enclave's margin and in particular on the left side where the enclaves form a buttress. In the *circle* there is a microgranular enclave and a cordierite-rich area. The *black arrow* indicates a felsic enclave. Hammer is 43 cm long

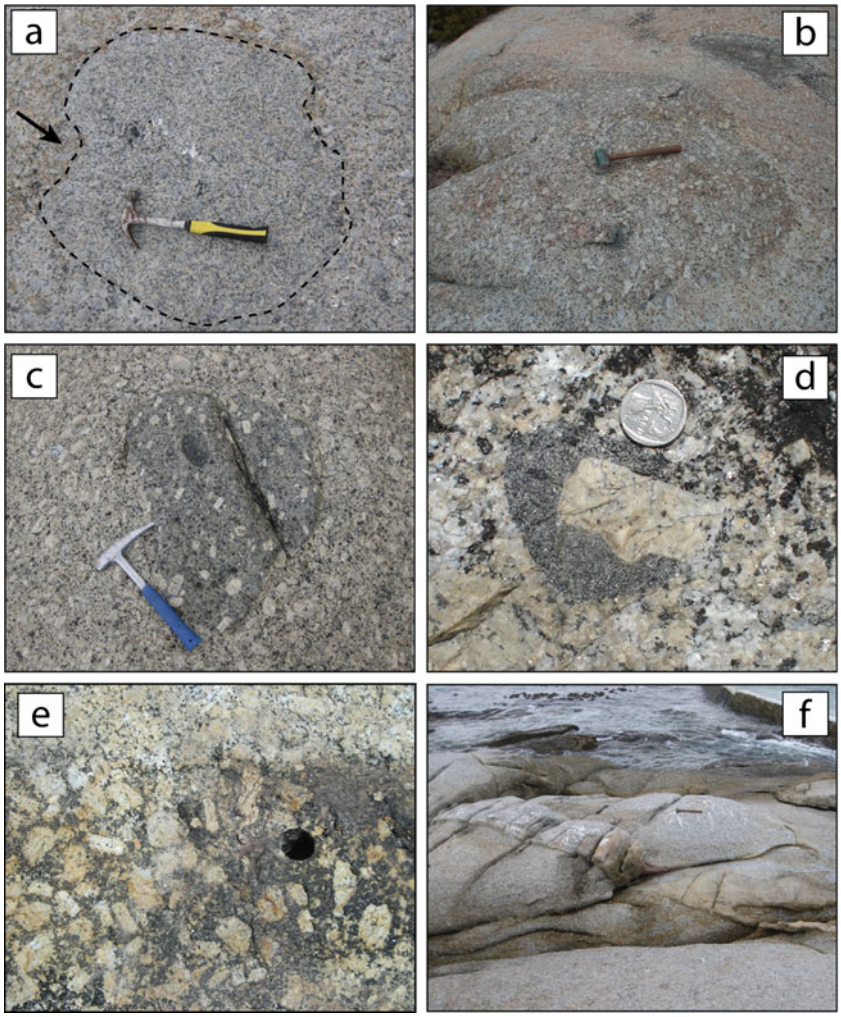

Fig. 6 Field photographs of enclaves and dikes: **a** Megacryst-free enclave; the *black arrow* indicates an indentation in the enclave. Hammer is 34 cm long. **b** Large porphyritic granodiorite enclave. Hammer is 43 cm long. **c** Porphyritic granodiorite enclave. Hammer is 32 cm long. **d** Microgranitoid enclaves with large alkali feldspar megacryst straddling the enclave-host boundary. Coin diameter is 2 cm. **e** Coarse-grained mafic enclaves. Drilled core diameter is 6 cm. **f** Zoned leucogranitic dike. The dike is characterized by an internal transition between a medium-grained external zone and a coarse-grained megacrysts-bearing internal part. Hammer is 43 cm long

and biotite occurs in some granodioritic enclaves. The groundmass is made up of quartz, plagioclase, biotite and minor K-feldspar. Porphyritic granodiorite enclaves have rounded shape, have sharp contacts with the host granite and range in size from 20 cm to 3 m in diameter (Fig. 6b, c). Large enclaves are composite and commonly host mafic microgranitoid enclaves and metamorphic xenoliths.

Microgranitoid enclaves have ovoid to sub-spherical shapes, diameters of less than 30 cm and are darker in colour than their host (Fig. 6d). The enclaves are typically fine grained and have equigranular, weakly poikilitic igneous microstructures. They are tonalitic to granodioritic and mostly dominated by the assemblage plagioclase, biotite, quartz and K-feldspar. K-feldspar megacrysts from the host may have been physically incorporated into the microgranitoid enclaves (Fig. 6d). K-feldspar megacrysts may straddle the enclave-host boundary and they do not present evidence for chemical interaction with the surrounding enclave suggesting late incorporation. Microgranitoid enclaves are rare in the pluton.

Coarse-grained mafic enclaves are rounded to bean-shaped bodies with dimensions ranging from 0.5 to 1 m and contain abundant large pseudomorphs of cordierite replacing former garnet as well as fine-grained symplectitic clots of biotite and quartz. They mostly consist of cordierite, biotite, quartz and plagioclase with almandine-rich garnet commonly preserved in the pseudomorphs. Occasionally, they may contain up to 30 vol.% of K-feldspar megacrysts similar in size and texture to those in the host granite (Fig. 6e). In the enclaves, the relative modal abundance and size of cordierite pseudomorphs, biotite + quartz clots and plagioclase is strongly variable. Accessory phases are apatite, zircon, ilmenite, monazite and rare titanite. It is noteworthy that cordierite in the pseudomorph is pinitized by a mineral assemblage involving biotite, white mica and kaolinite. The occurrence of a K-free phyllosilicate such as kaolinite, generally at the core of cordierite pseudomorphs, is characteristic of coarse-grained mafic enclaves.

Leucogranitic dikes crop out mainly on the eastern coast south of Simon's Town (Fig. 1). The leucogranites are fine- to medium-grained and have syenogranitic to monzogranitic composition. The dikes have width varying between 20 cm and 6 m. Thin dikes are generally equigranular and fine-grained while thick ones are texturally and compositionally

zoned (Fig. 6f). The external margin of zoned dikes is leucocratic and fine-grained, while the inner part is medium-grained and characterized by K-feldspar megacrysts, plagioclase, quartz and large cordierite crystals set in a fine-grained groundmass. Within zoned dikes the contacts between different zones vary from sharp to transitional. Thin homogeneous dikes sporadically cut K-feldspar megacrysts accumulations showing evidence of segregation from the surrounding magmatic structures.

Finally, metasedimentary xenoliths are widespread within the Peninsula pluton and have sizes ranging between 3–4 cm and 30 cm in length. Their concentration in the pluton is variable but on average 1 xenolith every 5 m^2 is observed. Metamorphic mineral assemblages in the xenoliths range in grade from lower greenschist facies up to garnet-bearing amphibolite facies. Low metamorphic grade xenoliths commonly preserve their original sedimentary bedding while those in amphibolite facies have metamorphic fabrics defined by biotite preferential orientation. Two different types of garnet-bearing metasedimentary xenoliths have been recognized and described by Villaros et al. (2009b): a biotite-dominated metapelite and a quartz and feldspar-dominated metapsammite. Both xenolith types contain a well-developed foliation defined by aligned biotite crystals and continuous quartzo-feldspathic layers with a metamorphic texture, both of which wrap garnet crystals. Garnet-biotite thermometry (Holdaway 2000) produces temperature estimates of 715°C and 735°C (±25°C) respectively for the metapelitic and metapsammitic xenoliths (Villaros et al. 2009b).

Magmatic structures

The Peninsula pluton is characterized by a wide range of mesoscopic magmatic structures that are similar to those described for other monzogranitic-granodioritic plutons worldwide (e.g. Barrière 1981; Clarke and Clarke 1998; Weinberg et al. 2001; Wiebe et al. 2007; Žák and Klomínsky 2007; Vernon and Paterson 2008; Paterson 2009). Magmatic structures are mostly defined by anomalously high concentrations of K-feldspar megacrysts, pseudomorphs of cordierite after garnet, biotite-quartz clots and biotite accumulation in schlieren. Magmatic structures have been subdivided into: K-feldspar megacryst-rich pipes, mafic mineral aggregates also containing K-feldspar megacrysts, xenoliths and magmatic enclaves, biotite-rich schlieren and sheeted structures such as layering and troughs (Figs. 7 and 8). It is not uncommon to find combinations of the above structures and gradations between them. In particular, biotite-rich schlieren are commonly associated with pipes and mafic aggregates and form the basal part of individual layers in sheeted

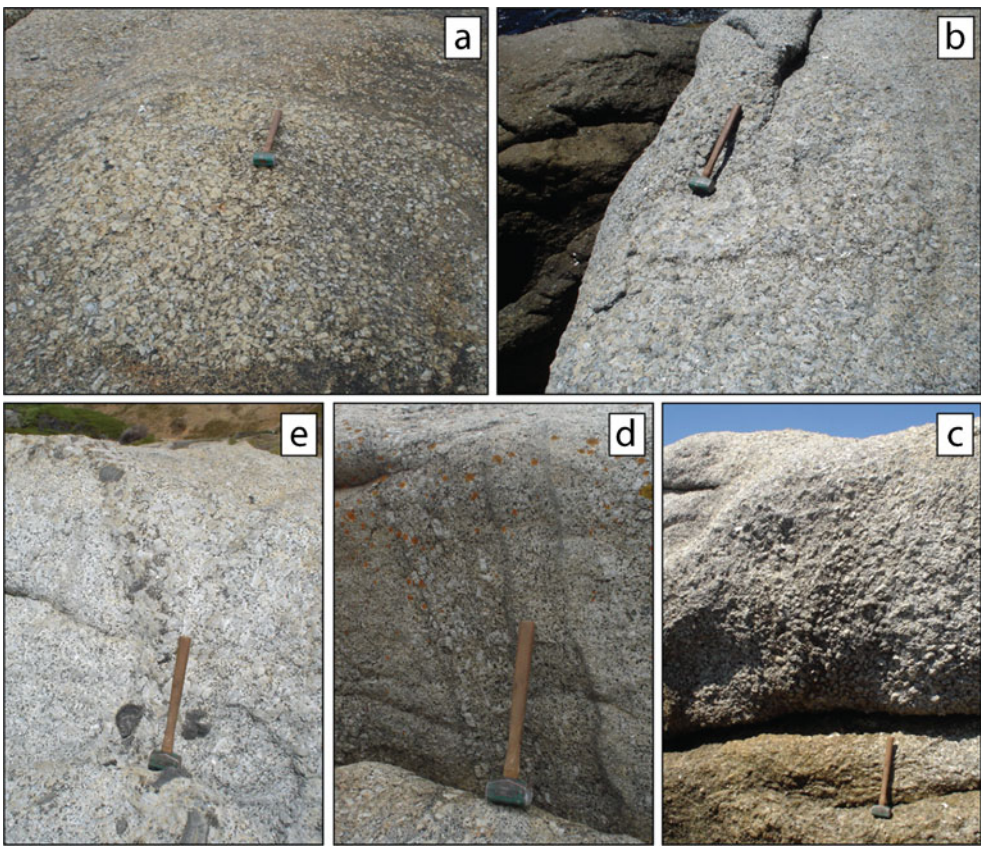

Fig. 7 Photographs of magmatic pipes. **a** Sub-horizontal surface through pipe, a single biotite-rich schlieren-like layer defines the outer pipe margin. **b**–**c** Horizontal and vertical surfaces through pipe, respectively. **d** Vertical surface through a small pipe formed in a finer-grained and megacryst-depleted variety of the pluton. Sub-vertical biotite schlieren define the outer pipe margin and mark different domains within the pipe. **e** Vertical surface through a small pipe containing microgranitoid enclaves, metamorphic xenoliths and cordierite-rich domains. The hammer for scale is 43 cm long

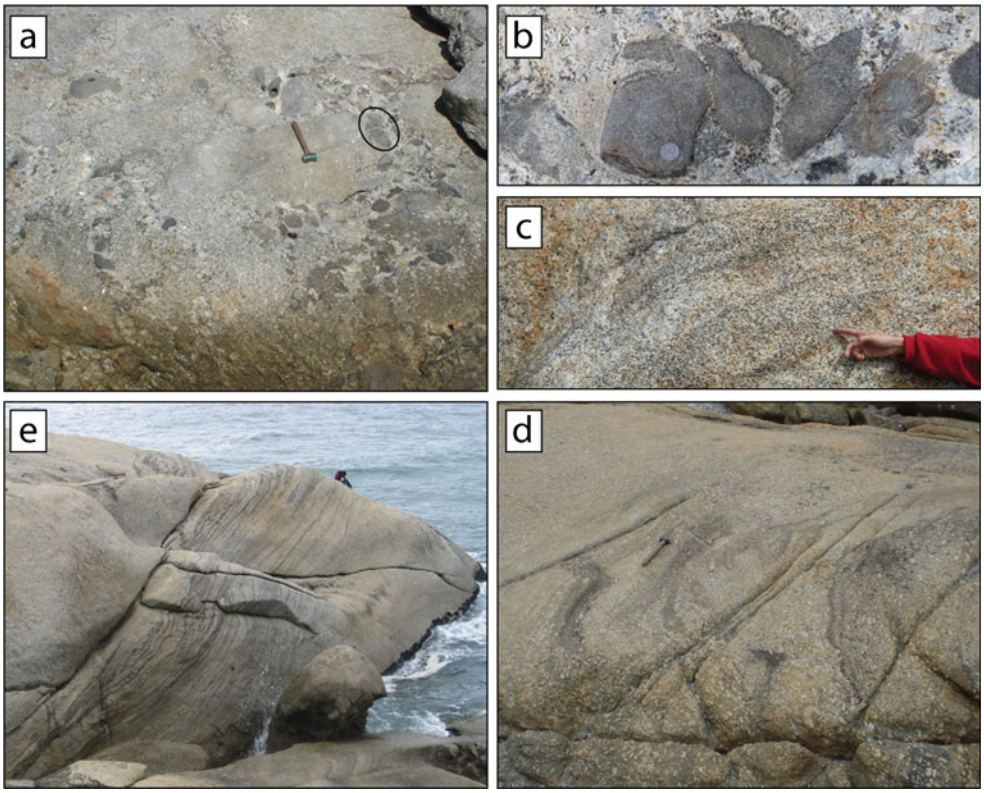

Fig. 8 Photographs of magmatic structures in the Peninsula pluton. (**a**) Mafic aggregate characterized by many texturally and compositionally variable microgranular enclaves and metamorphic xenoliths as well as by uneven distribution of K-feldspar megacrysts. Partially disaggregated microgranular enclaves are *encircled*. 43 cm long hammer for scale. (**b**) Close-up from figure (**a**) showing partially disaggregated enclaves. Coin diameter is 2 cm. (**c**) Biotite- schlieren. (**d**)–(**e**) Sheeted structures: trough (**d**) and general view of the Llundudno layering (**e**)

structures. Not all the structures occur with the same frequency: pipes are by far the most common feature in the pluton while rhythmic structures are rare and mostly occur in exposures of the pluton along the north-western coast.

Pipes are enclosed cylindrical-shaped accumulations of megacrysts commonly consisting of more than 70 vol.% of K-feldspar megacrysts and characterized by vertical or steeply plunging axis (Fig. 7a–e). The vertical extents of pipe structures can be demonstrated to exceed 5 m and are always greater than their sub-horizontal diameter that vary from few decimetres to a maximum of 3 m. Pipe diameters are generally constant along their sub-vertical axes (Fig. 7c–e). K-feldspar megacrysts in the pipes are similar to those in the host granite in size, shape and internal structure, showing inclusions of biotite along concentric growth rings. Megacrysts can be imbricated and some of them touch without moulding. The pipes contain all the minerals observed in the surrounding host magma and may also include mafic microgranitoid enclaves and metamorphic xenoliths (Fig. 7e). Some pipes have a single, weakly developed biotite-rich schlieren-like layer along the outer pipe margin (Fig. 7a). In a minority of cases, the biotite-rich schlieren and megacryst-rich layers alternate perpendicular to the main sub-vertical axis generating a structure defined by concentric tubes (Fig. 7d; e.g. Paterson 2009). It is noteworthy that megacryst abundances in host magmas are neither depleted nor enriched as pipes are approached. Pipes are generally spatially clustered and their density locally reaches 5 pipes every 100 m^2.

Mafic mineral aggregates consisting of cordierite, biotite-quartz clots and K-feldspar megacrysts and bearing abundant xenoliths and microgranular-granodioritic enclaves are widespread throughout the pluton (Fig. 8a). These aggregates have irregular three-dimensional shapes and occupy areas from 1 to up to 30 m^2. The contacts between the aggregates and the host granites vary from sharp to diffuse and can be occasionally marked by biotite-rich schlieren. Within individual aggregates the relative abundance of K-feldspar megacrysts and ferromagnesian phases is strongly variable and these phases commonly form separate domains exhibiting sharp internal contacts. Magmatic enclaves and metamorphic xenoliths are significant components and they may be locally clustered forming up to 50 % of the aggregates (Fig. 8a). Enclaves and xenoliths show contrasting dimensions, textures and compositions suggesting different wall-rock sources for xenoliths and different sources and/or degree of mingling-mixing for the magmatic enclaves. Magmatic enclaves may present evidence of incipient disruption and deformation indicating that, at the time the aggregate formed, they were not completely solid (Fig. 8b). In some cases, megacrysts appear to have been concentrated at the margins of enclaves and xenoliths.

Planar to curved biotite-rich schlieren are sparsely distributed in the Peninsula pluton. Schlieren form the basal mafic layers within sheeted structures, occur along the

margins of pipes and are also commonly found as isolated features (Fig. 8c). Some schlieren are wispy, folded and highly irregular in shape and are generally only continuous over a few meters while others are more planar and laterally continuous. They can be modally graded showing sharp bottoms and diffusive tops and their width varies between few centimetres to tens of centimetres. In sheeted structures schlieren are commonly associated with K-feldspar megacrysts showing preferential alignment parallel to the schlieren margin. Schlieren are not associated to magmatic enclaves or xenoliths.

Sheeted structures are formed by the repetition of zoned layers with thicknesses ranging from 10 cm to 1 m. Every individual layer is formed by a schlieren-like base grading to a leucocratic upper part dominated by plagioclase, K-feldspar and quartz. Cordierite crystals are commonly concentrated in the bottom part of the leucocratic sub-layer. K-feldspar megacrysts commonly show preferential alignment parallel to the layering in the schlieren but much weaker alignment in the leucocratic sub-layers. According to their geometry, sheeted structures have been subdivided into troughs and layering (Fig. 8d and e, respectively). Magmatic layering is symmetrical and defined by planar layers while troughs have been defined by Paterson (2009) as open, asymmetrical schlieren bounded curved channels whose repetition pattern is more irregular than that characteristic of layering. Sedimentary-like structures such as laminations, apparent erosion surfaces, load-casts and flames characterize sheeted structures. Sheeted structures are extremely rare in the pluton, essentially cropping out in two localities on the coast between Llandudno and Sea Point, and they will not be described any further in this contribution.

Whole-rock chemical variability

Sixty-seven samples from the Peninsula pluton have been analyzed for major and trace element composition. Data for 40 samples are from Villaros et al. (2009a, b), whereas the remaining 27 analyses are from this work. All rock samples from the database have been subdivided on the basis of their field occurrence and mineralogy into the classification of rock and structural types presented above. The samples are representative of the compositional variability within the pluton and include: 41 samples from the main rock type, 4 leucogranitic enclaves, 3 megacryst-free enclaves, 4 porphyritic granodiorite enclaves, 3 microgranitoid mafic enclaves, 4 mafic mineral rich enclaves and 8 leucogranitic dikes. A selection of data is presented in Table 1; the complete database is available in the data repository. In addition, the Nd isotopic composition of 22 samples has been analyzed (Table 2). The main chemical features of the pluton have been already portrayed by Villaros et al. (2009a, b). In this section we will briefly review the chemical variability of the Peninsula pluton as a whole and then we will focus on the chemical diversity exhibited by the volumetrically dominant main rock type (hereafter the Peninsula monzogranite) as well as by enclaves and leucogranitic dikes according to the new classification of the igneous products presented.

The pluton is a magnesian, alkali-calcic peraluminous granite that exhibits an extreme range of major- and trace-element variability (e.g. SiO_2 60–80 wt.%, MgO 0.2–3.8 wt.%, K_2O 2.2–7.5 wt.%, Al_2O_3 10.4–17.1 wt.%). The rocks of the Peninsula pluton produce good quasi-linear positive correlations between MgO + FeO^T and TiO_2 (R^2= 0.93), MnO, P_2O_5 (R^2=0.79), Zr (R^2=0.89), Nb and Th (Figs. 9 and 10) and non-linear positive correlations between MgO + FeO^T and A/CNK, heavy rare earths and Y. Moreover, CaO and Mg# (i.e. Mg# = Mg/(Mg + Fe)) are positively correlated with MgO + FeO^T up to the values characteristic of microgranitoid enclaves (≈9.0 wt.%) while coarse-grained mafic enclaves have a less calcic and magnesian character and show an internal negative correlation between CaO and MgO + FeO^T. Considering the subset of samples that form the Peninsula monzogranite in isolation, these rocks are strongly peraluminous (A/CNK 1.2–1.4) and shows a broad range of major and trace element variability (SiO_2 75–64 wt.%, MgO + FeO^T 3.4–8 wt.%, K_2O 3.3–6.4 wt.%, Al_2O_3 13.5–16.4 wt.%). When data are plotted over MgO + FeO^T: TiO_2, P_2O_5 and Zr form good positive linear correlations while alkalies, CaO, Mg#, Sr, Ba and Rb are extremely scattered showing a great degree of variation at any given MgO + FeO^T value. It is noteworthy that of the 41 samples analyzed the great majority show a limited variation in MgO + FeO^T (i.e.3.1–5.1) while four samples are remarkably more mafic (MgO + FeO^T 5.8–8.2) and TiO_2-rich. The monzogranite, leucogranitic dikes, megacrysts-free and coarse-grained mafic enclaves have $\varepsilon_{Nd(540)}$ ranging from −4 to −5 (Fig. 11).

Microgranitoid enclaves are highly peraluminous (A/CNK 1.3-1.6), have higher MgO, FeO^T and CaO and lower SiO_2 and K_2O content than the host monzogranite and do not plot on most of the linear trends defined by the host. In fact, relative to their MgO + FeO^T composition they are depleted in Nb, Y, Zr, Th and enriched in SiO_2. Moreover, in spite of their uniform MgO + FeO^T composition, microgranitoid enclaves have highly variable TiO_2 content. The microgranitoid enclaves consistently show higher $\varepsilon_{Nd(540)}$ (≈ −3) than the host granite and other enclaves. Porphyritic granodiorite enclaves are slightly more ferromagnesian and less SiO_2-rich than the greater part of samples from the monzogranite. Their $\varepsilon_{Nd(540)}$ (−3.4 to −4.2) overlaps with that of the monzogranite and microgranular enclaves.

The major and trace element composition of megacrysts-free enclaves is almost identical to that exhibited by the monzogranite. In spite of the lack of K-feldspar megacrysts,

Table 1 Representative whole-rock composition of granitoids of the Peninsula pluton

Rock type	Peninsula monzogranite						Microgranitoid enclave		Felsic enclave		Megacrysts-free enclave		Coarse-grained mafic enclave		Leucogranitic dykes			Porphiritic granodiorite enclaves	
Sample	PG10	PG12	PG13	PG3	PG6	BB	PG14-15	BB02A	OLD3	PG19	PG11	PG 24	PG22	PL9	PG25	PG28	PG8	PG21	PG23
wt %																			
SiO_2	68.46	68.53	69.59	69.72	69.61	64.30	70.05	67.26	73.59	76.62	75.30	70.62	63.91	62.27	70.42	75.35	72.96	67.83	69.19
TiO_2	0.47	0.54	0.50	0.46	0.45	1.04	0.90	0.83	0.17	0.36	0.43	0.48	1.22	1.85	0.22	0.22	0.07	0.72	0.58
Al_2O_3	15.56	15.81	15.04	14.48	14.68	15.27	12.36	14.48	14.14	11.06	11.97	14.32	13.79	12.08	15.09	12.58	14.91	14.42	14.34
FeO_T	3.11	3.03	3.17	2.93	3.07	4.48	4.94	5.50	1.28	2.29	2.88	2.81	7.24	10.59	1.65	1.91	0.51	4.19	3.65
MnO	0.05	0.05	0.05	0.05	0.05	0.07	0.06	0.06	0.03	0.04	0.05	0.04	0.13	0.20	0.03	0.04	0.01	0.07	0.07
MgO	1.04	1.02	1.08	1.00	0.89	2.08	2.44	2.35	0.41	0.68	0.92	0.89	2.71	3.68	0.45	0.47	0.17	1.50	1.28
CaO	1.30	1.36	1.47	1.30	1.36	0.56	1.55	2.02	0.82	0.67	0.94	1.54	1.69	1.11	0.72	0.55	0.44	1.84	1.56
Na_2O	2.87	3.02	2.88	2.73	3.11	1.94	2.38	2.68	2.94	2.07	2.31	3.06	2.07	1.00	2.73	2.30	3.39	2.59	2.78
K_2O	5.45	5.30	4.99	4.65	5.04	4.63	2.67	2.24	5.89	4.68	4.23	4.68	3.23	3.98	6.80	5.38	7.20	4.43	4.13
P_2O_5	0.23	0.24	0.22	0.21	0.21	0.25	0.18	0.19	0.12	0.19	0.22	0.17	0.28	0.50	0.17	0.18	0.15	0.29	0.21
LOI	1.06	1.00	0.97	1.33	1.09	1.98	1.44	1.40	0.68	0.63	1.02	1.04	2.61	1.60	0.92	0.90	0.85	1.36	1.91
total	99.60	99.90	99.96	98.86	99.56	96.60	98.97	99.01	100.08	99.29	100.27	99.65	98.88	98.86	99.20	99.88	100.66	99.24	99.70
MgO + FeO	4.15	4.05	4.25	3.93	3.96	6.56	7.38	7.85	1.69	2.97	3.80	3.70	9.95	14.27	2.10	2.38	0.68	5.69	4.93
A/CNK	1.20	1.20	1.17	1.22	1.12	1.66	1.28	1.38	1.11	1.13	1.19	1.11	1.38	1.52	1.15	1.19	1.05	1.16	1.21
Mg#	0.37	0.38	0.38	0.38	0.34	0.45	0.47	0.43	0.37	0.35	0.36	0.36	0.40	0.38	0.33	0.30	0.37	0.39	0.38
ppm																			
V	46	47	46	44	44		117		17	33	42	41	132	175	20	14	7	72	58
Cr	34	37	33	35	33		87		21	29	32	17	70	97	16	14	17	38	30
Ni	26	20	20	21	20		40		14	17	19	13	32	51	10	35	13	20	17
Zn	71	68	67	63	65		86		38	56	71	72	143	184	54	40	16	82	86
Rb	282	270	257	250	284	362	230	195	248	255	252	245	230	385	276	283	289	254	268
Sr	91	89	85	81	78	92	104	79	89	42	45	103	106	37	114	33	30	100	94
Y	28	31	27	28	30	54	25	35	27	35	35	23	51	127	24	38	12	34	33
Zr	168	173	183	175	179	353	236	215	86	134	156	176	488	878	97	109	39	241	221
Nb	19.0	19.5	18.8	18.8	19.3	31.3	15.2	18.1	6.4	16.3	19.5	19.1	35.8	73.4	11.5	13.1	4.4	23.0	20.1
Ba	481	410	381	334	384	231	697	135	410	141	122	554	504	204	1006	47	83	372	400
La	31	31	34	32	30	63	36	39	15	26	27	35	81	129	18	16	5	40	39
Ce	71	71	78	74	69	127	75	74	31	61	63	76	166	255	41	39	13	86	85
Pr	7.7	7.7	8.4	7.9	7.5		8.6		3.5	6.6	6.8	8.4	19.7	31.3	4.5	4.4	1.3	9.7	9.4
Nd	30	29	32	30	30	56	35	33	14	25	27	30	78	130	17	17	5	38	38
Sm	6.4	6.4	7.2	6.4	6.3	12.4	7.2	7.0	3.1	5.8	5.6	6.2	16.1	27.2	4.0	4.6	1.5	7.6	7.8
Eu	1.0	1.0	0.8	0.8	0.9	1.0	1.2	0.9	1.0	0.4	0.5	1.1	1.3	0.6	1.3	0.4	0.3	1.0	0.9
Gd	5.5	5.5	5.5	5.6	5.6	11.8	6.3	6.6	2.9	5.1	5.9	5.1	12.9	24.3	3.6	5.0	1.5	7.4	6.8
Tb	0.85	0.88	0.85	0.97	0.93	1.85	0.87	1.02	0.56	0.92	0.96	0.76	1.78	3.61	0.63	0.90	0.28	1.08	1.04

Table 1 (continued)

Rock type	Peninsula monzogranite						Microgranitoid enclave		Felsic enclave		Megacrysts-free enclave		Coarse-grained mafic enclave		Leucogranitic dykes			Porphiritic granodiorite enclaves	
Sample	PG10	PG12	PG13	PG3	PG6	BB	PG14-15	BB02A	OLD3	PG19	PG11	PG 24	PG22	PL9	PG25	PG28	PG8	PG21	PG23
Dy	5.3	5.7	5.5	5.5	5.6	11.4	5.2	6.4	4.2	6.4	6.6	4.5	10.4	24.3	4.6	7.0	2.1	6.8	6.7
Ho	0.92	1.13	0.97	0.99	1.15	1.87	0.90	1.28	1.01	1.25	1.22	0.90	1.90	4.71	0.78	1.32	0.40	1.24	1.23
Er	2.78	3.15	2.65	2.59	3.36	5.00	2.29	3.52	3.29	3.55	3.47	2.43	5.16	14.22	2.19	3.64	1.18	3.58	3.10
Tm	0.41	0.42	0.42	0.38	0.51	0.73	0.33	0.46	0.55	0.46	0.51	0.34	0.71	2.01	0.31	0.53	0.18	0.51	0.42
Yb	2.48	2.89	2.40	2.44	3.27	4.67	1.72	3.03	3.56	3.08	3.20	2.55	4.71	13.33	1.94	3.05	1.15	3.13	2.56
Lu	0.37	0.39	0.33	0.34	0.47		0.31		0.59	0.39	0.44	0.33	0.69	1.92	0.25	0.39	0.16	0.43	0.32
Hf	4.5	4.8	4.8	4.7	4.8	9.3	6.1	6.0	2.8	3.7	4.4	4.4	12.7	23.0	2.9	3.5	1.5	6.3	5.7
Ta	1.80	1.70	1.64	1.63	1.59		0.95		0.61	1.77	1.91	1.34	2.67	5.57	0.99	1.18	1.06	1.81	1.64
Pb	36	34	33	33	34		14		47	29	25	47	17	7	66	40	37	33	29
Th	15.1	14.7	16.3	15.9	14.7	28.0	10.3	16.0	7.5	14.9	14.3	15.8	34.9	64.0	9.7	11.5	4.4	17.4	18.7
U	8.3	11.4	7.7	6.6	7.9		4.0		4.1	8.1	7.5	4.6	3.4	18.4	3.3	4.8	5.1	6.9	5.9

their average K_2O composition (4.4 wt.%) is just slightly lower than that of the main rock type (4.9 wt.%). In addition, the three samples analyzed are on average less aluminous (Al_2O_3 = 13.3 wt.%) than the monzogranite. Coarse-grained mafic enclaves are the most ferromagnesian (MgO + FeO^T 11.1–15.6 wt.%) and TiO_2-rich and have the lowest SiO_2 and Na_2O of all rocks in the pluton. They are strongly peraluminous and have higher REE content. The trace element content of mafic enclaves is strongly variable and two groups can be distinguished. The two less ferromagnesian samples have higher Sr, Ba and lower Rb, Y, Nb, Th than those more FeO^T- and MgO-rich.

Leucogranitic dikes and leucogranitic enclaves are slightly peraluminous with average SiO_2 content of 75 wt.% and low FeO^T, MgO and TiO_2. K_2O is high and varies from 4.4 to 7.4 wt.%; CaO is always lower than 1 wt.% Leucogranitic rocks in the pluton are depleted in those elements that are concentrated within zircon and monazite (La, Ce, Yb, Zr, Th and Hf) as well as in large ion lithophile elements.

The occurrence of very large alkali-feldspar crystals in the pluton may raise doubts about the representativeness of the samples collected. In fact, although coarse-grained, the pluton has a porphyric appearance due to the much bigger size reached by alkali-feldspar with respect to the other phases in the rock. Therefore, it may be argued that the major and trace element chemical variability described for the pluton reflects the relative proportion of alkali-feldspar megacrysts and "matrix" that happen to be analyzed in samples that are too small to be representative of the rock composition. This hypothesis can be easily discarded. In fact, the abundance of megacrysts in the rock is inadequate to justify the variability in the ferromagnesian component exhibited by the pluton. The good positive linear correlation between MgO + FeO_{tot} and TiO_2 may form by collecting rock samples that contains approximately 50 wt.% less (or more) alkali-feldspar megacrysts than a hypothetical representative samples having the average composition of the pluton. This is clearly inconceivable because it would translate into K_2O contents that are negative for the more ferromagnesian rocks and up to 10 wt.% for the more leucocratic samples.

Mineral chemistry

K-feldspar megacrysts

Analyses of individual spots within three selected megacrysts were carried out on polished core to rim surfaces cut perpendicular to the (010) Carlsbad twin plane (Table 3). The major element composition in the core region of the two megacrysts from the monzogranite varies between 80 and 95 mol % Or while the rim has a more limited range of

Table 2 Nd isotope data for the Peninsula pluton

Sample	Rock type	Sm ppm	Nd ppm	$^{143}Nd/^{144}Nd_{(m)}$	±2σ	$^{147}Sm/^{144}Nd$	$^{143}Nd/^{144}Nd_{(540)}$	ε_{Nd}	Error
BB08	mz	7.4	35.8	0.512141	9	0.12554	0.51170	−4.8	0.66
MP01	mz	6.5	30.4	0.512159	9	0.12898	0.51170	−4.7	0.68
OK07	mz	6.0	26.1	0.512223	9	0.13836	0.51173	−4.1	0.74
PG 03	mz	6.4	30.1	0.512193	12	0.12893	0.51174	−4.0	0.68
PG 12	mz	6.4	29.4	0.512162	9	0.13241	0.51169	−4.9	0.7
CB 103	mz	6.2	30.9	0.512153	14	0.12148	0.51172	−4.3	0.64
SB 01	mz	6.2	30.9	0.512158	15	0.12223	0.51173	−4.2	0.81
SB 03	mz	6.2	27.8	0.512185	9	0.13481	0.51171	−4.6	0.72
PG 11	mf	5.6	26.7	0.512179	11	0.12746	0.51173	−4.2	0.67
PG 24	mf	6.2	30.0	0.512161	8	0.12579	0.51172	−4.4	0.66
PG 14-15	mgr	7.2	35.5	0.512235	10	0.12226	0.51180	−2.7	0.64
BB01	mgr	10.6	50.3	0.512232	12	0.12771	0.51178	−3.2	0.67
BB11	pgr	10.1	50.6	0.512154	8	0.12058	0.51173	−4.2	0.63
PG 21	pgr	7.6	38.4	0.512198	9	0.11917	0.51178	−3.2	0.62
PG 23	pgr	7.8	38.0	0.512210	22	0.12472	0.51177	−3.4	0.66
BB12	lg dyke	2.8	9.8	0.512282	9	0.16930	0.51168	−5.1	0.93
PG 25	lg dyke	4.0	16.6	0.512232	11	0.14457	0.51172	−4.3	0.78
PG 26	lg dyke	7.1	28.9	0.512255	10	0.14872	0.51173	−4.2	0.8
OLD 03	lge	3.1	13.9	0.512195	15	0.13394	0.51172	−4.3	0.71
PG 20	lge	3.8	17.4	0.512217	12	0.13097	0.51175	−3.7	0.69
PL 9	cgm	27.2	130.0	0.512171	7	0.12701	0.51172	−4.3	0.67
PG 22	cgm	16.1	78.4	0.512135	11	0.12398	0.51170	−4.8	0.65

mz Peninsula monzogranite, *mf* megacryst-free enclaves, *mgr* microgranitoid enclaves, *pgr* porphyritic granodiorite enclaves, *lg dyke* leucogranitic dykes, *lge* leucogranitic enclaves, *cgm* coarse-grained mafic enclaves

mol % Or (82–86) than the core. The third megacryst comes from a porphyritic granodiorite enclave and displays a similar range of Or mol %. However, this sample is characterized by an abrupt change in the Or content (96–79 mol %) across a sharp xenomorphic resorption plane marked by an increased abundance of mineral inclusions rimward.

Biotite

Biotites from the monzogranite as well as from felsic, microgranular, porphyritic granodiorite and coarse-grained mafic enclaves have been analyzed (Table 4, Electronic Supplementary Material) and presented in Fig. 12. Distinct textural types of biotite are recognised in the monzogranite: coarse- to medium-grained biotite crystals, small biotites hosted in K-feldspar megacrysts, biotite forming biotite-quartz clots and inclusion-poor elongated biotite crystals associated with muscovite in pinite. Biotite in the clots, individual biotites and crystals hosted in K-feldspar megacrysts display a limited range in Mg# (0.31-0.37) while biotite in pinite is consistently more Mg-rich (Mg# 0.37-0.43) and contains less Ti; both characteristics being consistent with a low temperature origin. Microgranitoid enclaves are characterized by two different biotite compositions: crystals in the enclave's core are strongly more magnesian (Mg# 0.48-0.54); Al^{VI}-rich and (1.1-1.3 apfu) lower in K (≈1.6 apfu) than biotites in the rim (Mg# 0.37-0.41, Al^{VI} 0.9-1.1 apfu, $K \approx 1.7$ apfu). Biotites in the rim have compositions converging toward those characteristics of biotites in the monzogranite. Although, biotites of the granodioritic enclaves and those characterizing the rim of microgranitoid enclaves have identical Mg#, the latter are higher in Al^{VI} and lower in K. Finally, biotites in felsic enclaves are most Fe- and K-rich.

Discussion

Incremental construction of the Peninsula pluton

Isotopic evidence presented by Villaros et al. (2011) and Harris and Vogeli (2010) suggest that the Peninsula pluton formed incrementally by amalgamation of magma batches whose isotopic composition is directly inherited from the source. Zircon grains from the pluton have been analyzed by Villaros et al. (2011) by LA-ICP-MS and LA-MC-ICP-MS

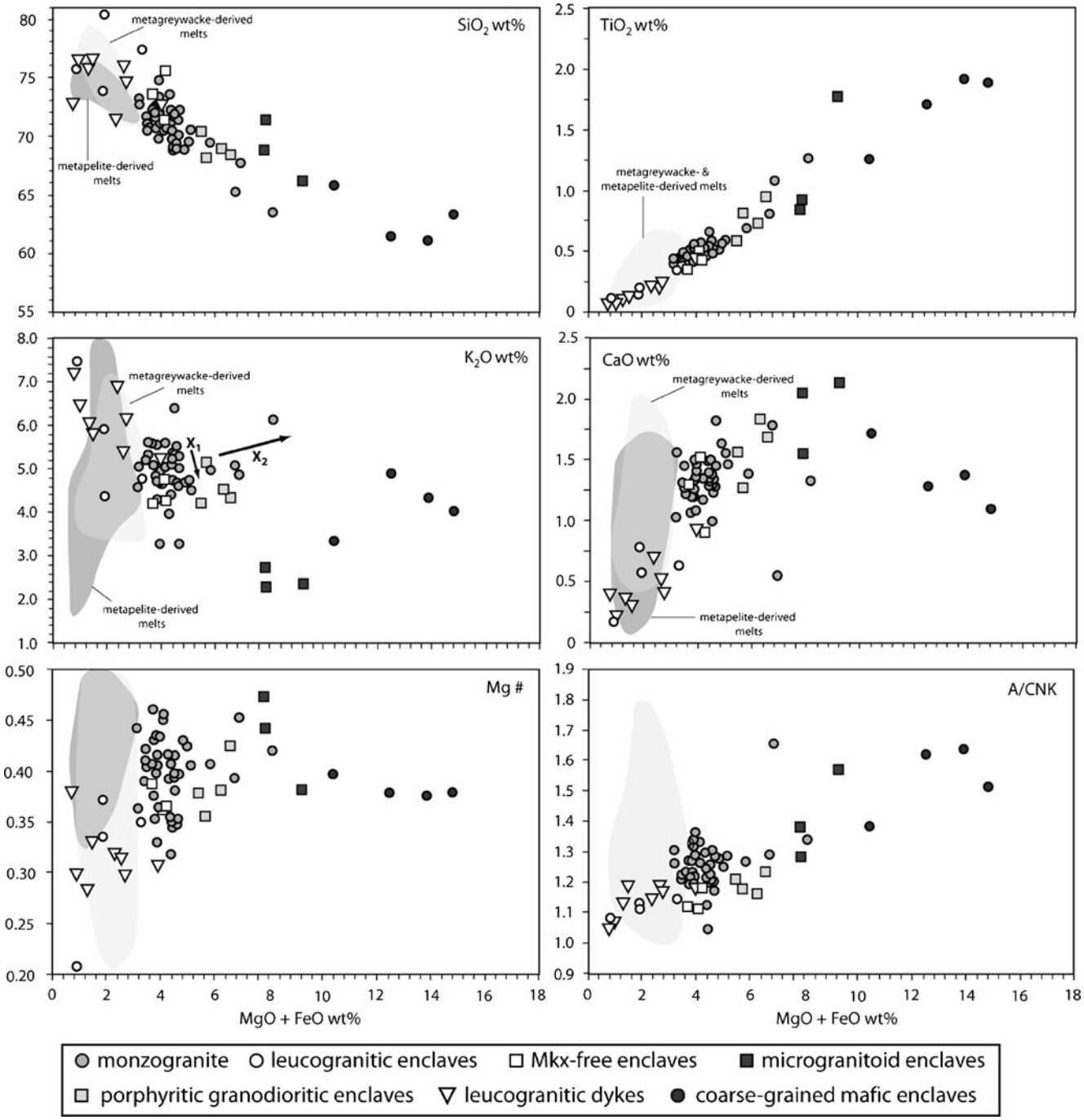

Fig. 9 Major element variation diagrams showing the compositional variations of the different rock types. Vector x_1 indicates removal of 10 vol.% of pipes from the average monzogranite composition, vector x_2 represents addition of 10 wt.% of biotite. Fields for experimental melts derived by fluid-absent melting of metagreywackes and metapelites at T <950°C are shown. Metagreywacke-derived melts are from Montel and Vielzeuf (1997); Stevens et al. (1997); Patiño Douce and Beard (1996); Gardien et al. (1995); metapelite-derived melts are from Vielzeuf and Holloway (1988); Stevens et al. (1997); Pickering and Johnston (1998); Patiño Douce and Johnston (1991); Patiño Douce and Harris (1998)

to determine their age and Hf isotopic composition. The inherited zircons have variable ε_{Hf} values providing evidence for an isotopically heterogeneous crustal source recording several regional events between 600 and 1,200 Ma. Within individual samples, magmatic and inherited zircons record similar ranges of initial ε_{Hf} (when both recalculated to the age of emplacement for the pluton). This has been interpreted to reflect transfer of the inherited zircon within small magma domains with no homogenization at larger scale. This lack of homogenization argues for the assembly

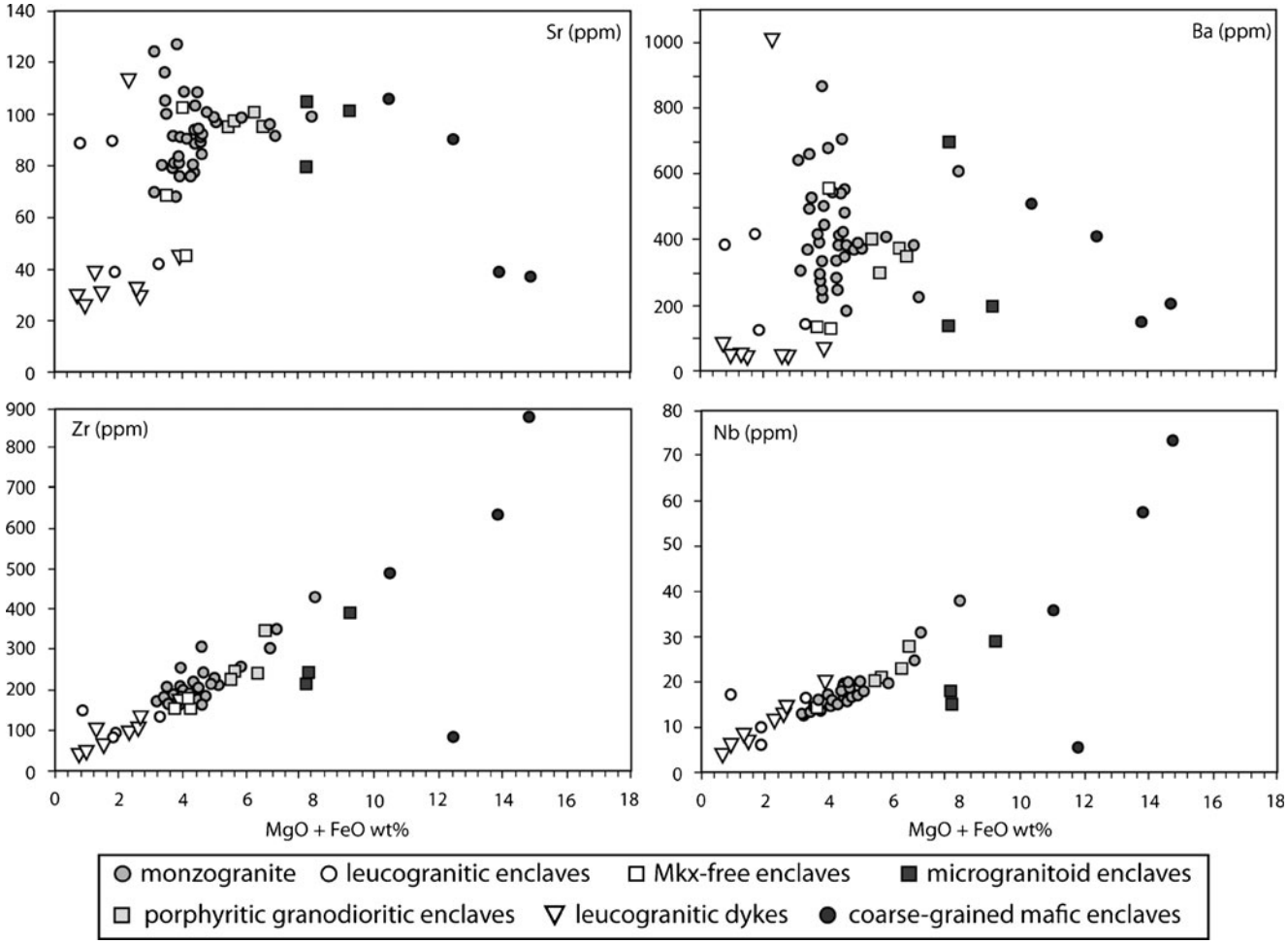

Fig. 10 Trace element variation diagrams showing the compositional variations between the different rock types

of the pluton through many relatively small magma batches that undergo rapid cooling from their initial temperature to the temperature at which much of the magmatic zircon had crystallized.

This interpretation is supported by the variable oxygen isotopic composition recorded by garnet in the pluton (from 10.0 to 11.4‰; Harris and Vogeli 2010). In fact, the high closure temperature of garnet (>810°C) to oxygen diffusion means that garnet $\delta^{18}O$ values would not have changed as a result of oxygen diffusion between the garnet, the magma and other phases. Therefore, garnet $\delta^{18}O$ variability is consistent with melting of a heterogeneous source to produce magma batches characterized by slightly different $\delta^{18}O$ values. Magma batches were subsequently mixed and partly homogenized before and/or during the emplacement process, resulting in a narrower spread of quartz $\delta^{18}O$ values (Harris and Vogeli 2010).

Although isotopic data support pluton growth by incremental emplacement of magma batches whose chemical composition is mostly inherited from the source, no simple and obvious field evidence for multiple magma injections is preserved in the pluton. The lack of sharp contacts between the inferred batches can result from two different scenarios: i) original sharp contacts produced by new magma into solidified magma could have been destroyed by re-melting due to the arrival of successive hot magma batches; ii) sharp contacts may never have existed due to the intrusion of new magma batches into a partly molten magma chamber. Annen (2011) has described the thermal evolution of incrementally emplaced magma bodies where the individual intrusions are horizontal (sills). The first sill to be emplaced is in contact with a cold country rock and thus crystallizes rapidly whereas, with time, successive sills thermally equilibrate with their surroundings at progressively higher temperatures. When, after an incubation time mainly depending on emplacement rate, the temperature of the system is above the solidus temperature for the sills, individual increments will retain residual melt. Depending on the balance between heat input from magma replenishment and heat loss to the surroundings, relatively melt-rich zones may expand far beyond the

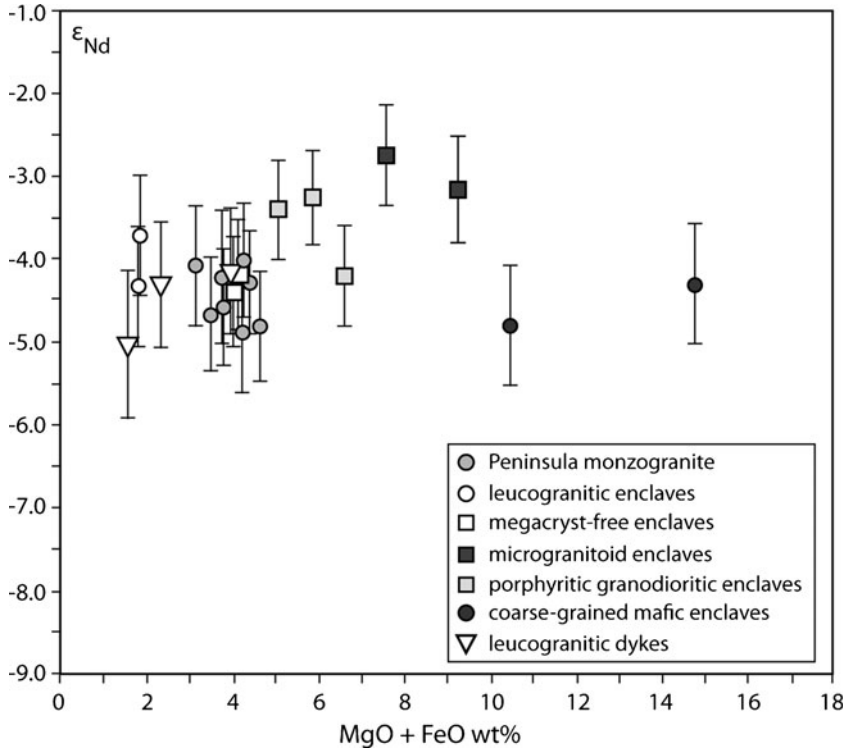

Fig. 11 ε_{Nd} (t) vs. MgO + FeO^T diagram showing the composition of the different rock-types in the Peninsula pluton. The Nd isotopic ratios have been corrected to 540 Ma. The error for ε_{Nd} (t) is calculated considering an uncertainty of 4 % on the Sm and Nd concentrations and an error of ±4 Ma on the age of the pluton

dimensions of individual sills precluding the development of sharp contacts between successive batches.

Timing of formation of magmatic structures

The magmatic structures in the Peninsula pluton present compelling evidence that they form by either concentration of crystals or removal of interstitial melt from crystal-rich mushes and not by in-situ growth. A list of this evidence follows: i) in pipes and mafic mineral aggregates, K-feldspar megacrysts are often imbricated without any internal deformation suggesting mechanical tilting during magmatic flow; ii) megacrysts are often in contact but they show no evidence of moulding of one crystal around another as would be expected in the case of metasomatic growth; iii) in sheeted structures and schlieren, megacrysts may locally define a dimensional preferred orientation, implying their movement as independent crystals suspended in the liquid; iv) the minerals in the magmatic structures are of about the same size as the equivalent minerals in the host; v) modal and grain size grading occur in some schlieren; this is consistent with deposition of crystals at a rheological boundary (e.g. Barrière 1981); vi) in mafic aggregates, magmatic enclaves and xenoliths of different varieties commonly concentrate (Fig. 8a) suggesting a connection between the process by which xenoliths, enclaves and associated megacrysts were concentrated. In these structures, microgranitoid enclaves may be moderately disrupted proving that they were still partially molten at the time of formation of the aggregate (Fig. 8b). In addition, alkali feldspar megacrysts and microgranitoid enclaves are occasionally concentrated on physical barriers formed by large felsic enclaves (Fig. 5). This evidence, together with the general lack of K-feldspar megacrysts in leucogranitic enclaves, attests to relative motion between leucogranitic enclaves and the megacrysts-bearing host magma, indicating that the enclaves were sufficiently crystallized to behave as rigid objects.

The timing and mechanism of formation of the magmatic structures occurring in the Peninsula pluton can be constrained by determining when and where in the magma plumbing system K-feldspar megacrysts crystallized. As they represent the prominent component of pipes and mafic aggregates and are commonly associated with schlieren and sheeted structures, these structures all formed following substantial megacryst crystallization. The origin of large K-feldspar crystals in granitic and granodioritic rocks has fascinated and puzzled petrologists for over a century. Although recently the dispute has been rekindled by the work of Johnson and Glazner (2009), who interpreted megacrysts to form by textural coarsening at sub-solidus conditions, there is generally a wide consensus within the scientific community on their magmatic origin (e.g. Vernon and Paterson 2008; Moore and Sisson 2008; Farina et al. 2010; Vernon 2010). Many textural and chemical lines of evidence shared by megacrysts from many different granitic to granodioritic plutons worldwide are commonly reported as evidence of their magmatic origin (e.g. Vernon and Paterson

Table 3 Representative core to rim data for K-feldspar megacrysts in the Peninsula pluton

Sample rim distance (mm)	PL6-A 19.3	PL6-A 18.4	PL6-A 16.6	PL6-A 12.5	PL6-A 9.8	PL6-A 6.1	PL6-A 5.2	PL6-A 2.6	PL6-A 1.2	PL6-B 14.5	PL6-B 11.2	PL6-B 8.3	PL6-B 6.2	PL6-B 2.3	PL6-B 1.3	BB11 14.6	BB11 7.3	BB11 0.9
SiO_2	66.22	66.10	65.98	66.46	66.23	65.98	66.04	66.19	65.99	65.48	65.50	65.37	65.19	65.78	66.09	64.19	64.41	63.95
Al_2O_3	19.15	18.84	18.92	19.13	19.10	18.97	19.04	19.06	18.89	18.80	18.76	18.81	18.78	18.90	18.91	18.63	18.66	18.47
Na_2O	2.30	0.92	0.66	2.45	2.15	1.41	2.18	2.48	1.48	1.12	2.01	1.64	1.36	1.62	1.81	0.96	2.00	0.34
K_2O	13.95	15.72	15.99	13.66	14.00	14.86	13.98	13.51	14.20	15.41	14.11	14.91	14.94	14.88	14.73	15.27	13.80	15.90
CaO	0.11	0.09	0.09	0.16	0.21	0.20	0.15	0.10	0.18	0.09	0.14	0.16	0.12	0.06	0.18	0.06	0.22	0.08
Total	101.73	101.67	101.64	101.86	101.69	101.42	101.39	101.34	100.74	100.90	100.52	100.89	100.39	101.24	101.72	99.11	99.09	98.74
Ab	0.202	0.083	0.060	0.216	0.190	0.126	0.192	0.217	0.136	0.100	0.178	0.143	0.121	0.143	0.158	0.086	0.177	0.031
Or	0.793	0.913	0.936	0.777	0.800	0.864	0.800	0.778	0.855	0.896	0.816	0.849	0.873	0.854	0.833	0.911	0.812	0.965
An	0.005	0.004	0.004	0.008	0.010	0.010	0.007	0.005	0.009	0.004	0.007	0.008	0.006	0.003	0.009	0.003	0.011	0.004

Table 4 Representative data for biotites in the Peninsula pluton

Rock type	Peninsula monzogranite							Microgranitoid enclave		Porphiritic granodiorite enclave			Coarse grained mafic enclave			Leucogranitic enclave		
Sample	PL6A-4	PL6A-4	PL6A-4	PL6A-4	PL 6A-6	ST10A	PL6- 1B	PG 14-15	PG 14-15	PL 23	PL 23	PL 23	BB 203B	BB 203B	BB 203B	OLD 03	OLD 03	OLD 03
Texture	*matrix-bt*	*matrix-bt*	*matrix-bt*	*matrix-bt*	*bt-qtz clot*	*bt-qtz clot*	*bt in Kfs*	*matrix-bt*	*matrix-bt*	*matrix-bt*	*matrix-bt*	*matrix-bt*	*bt pinite*	*bt-qtz clot*	*bt pinite*	*matrix-bt*	*matrix-bt*	*matrix-bt*
wt %																		
SiO_2	35.55	35.88	35.49	35.60	35.41	36.2	35.9	38.9	37.3	36.06	36.28	37.04	36.07	35.01	34.80	34.31	34.72	34.16
TiO_2	4.03	3.85	4.11	4.02	2.86	3.9	3.4	3.7	3.5	3.87	4.12	3.60	3.34	3.57	2.44	4.15	3.91	3.38
Al_2O_3	18.50	18.23	18.90	17.87	19.03	17.7	18.6	20.5	19.0	18.57	18.35	18.93	18.01	18.05	19.48	18.13	18.27	18.13
FeO	24.17	22.88	23.66	23.43	23.76	23.2	23.0	17.0	20.2	21.22	20.90	21.40	23.90	24.35	23.92	23.88	24.09	25.02
MnO	0.62	0.65	0.78			0.3	0.3		0.3	0.36	0.36	0.29	0.26	0.31	0.44	0.27	0.27	0.29
MgO	6.46	6.42	6.19	6.58	6.94	6.7	6.6	8.8	6.9	7.33	7.56	7.85	7.23	6.56	6.88	5.59	5.77	5.92
Na_2O		0.28	0.32			0.3	0.32							0.34	0.44			
K_2O	9.24	9.17	9.29	9.06	9.28	8.8	9.0	8.8	8.8	9.15	9.10	9.18	8.94	8.82	8.69	9.31	9.24	9.19
Total	98.57	97.35	98.73	96.56	97.28	97.21	97.07	97.65	95.96	96.55	96.67	98.29	97.73	97.01	97.10	95.62	96.28	96.09
Fe#	0.68	0.67	0.68	0.67	0.66	0.66	0.66	0.52	0.62	0.62	0.61	0.60	0.65	0.67	0.66	0.70	0.70	0.70

matrix-bt are coarse- to medium-grained individual crystals, *bt in Kfs* are biotites hosted in K-feldspar megacrysts

bt-qtz clot are biotites in the biotite-quartz clots and *bt pinite* are inclusion-poor crystals associated to muscovite in pinite

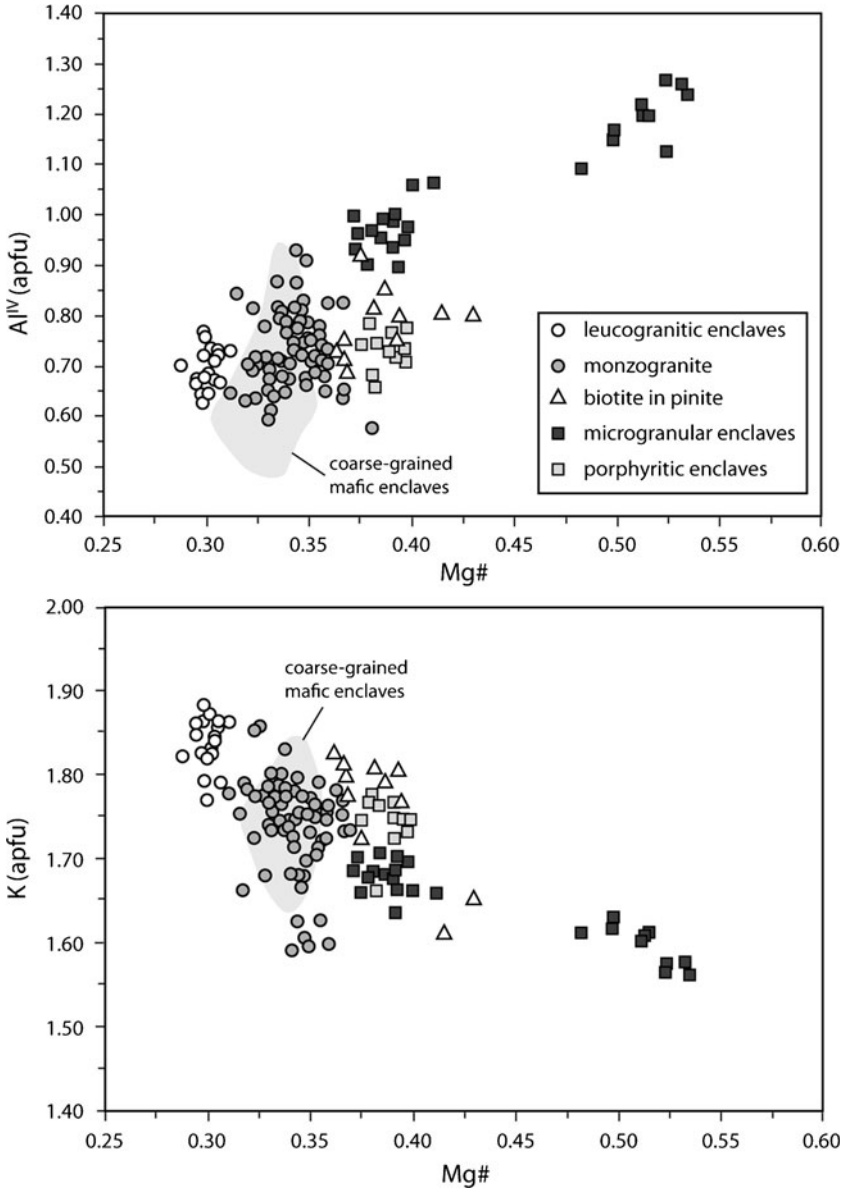

Fig. 12 Major element composition of biotites of the Peninsula pluton. In the key, coarse- to medium-grained individual biotite crystals, small biotites hosted in K-feldspar megacrysts and biotite forming biotite-quartz clots are all labelled "monzogranite". Mineral chemical formulae calculated on the basis of 22 cation charges. Mg# = Mg/(Fe + Mg)

2008). The textural and chemical evidence supporting their magmatic origin include: i) The crystals display major and trace element oscillatory zoning; ii) they host euhedral plagioclase and biotite crystals that are distinctly smaller (0.5–2 mm) than those in the framework of the rock (generally >3 mm); iii) they contain inclusions that are concentrically arranged parallel to crystallographic planes; iv) the occurrence of resorption surfaces in the megacrysts hosted in granodioritic enclaves as well as microgranitoid enclaves indented by megacrysts indicate that they were present before the microgranitoid and granodioritic enclaves crossed their solidi.

A crucial contribution to our understanding of when magmatic structures form is provided by experimental petrology studies which constrain the temperature at which K-feldspar starts to crystallize within appropriate magma compositions. Experimental data on both metaluminous (Piwinskii 1968) and peraluminous (Clemens and Wall 1981) granitic systems indicate that K-feldspar is the last rock-forming minerals to become saturated in the magma. In particular, in the experiments of Clemens and Wall (1981) K-feldspar starts to crystallize at 760–780°C in melts having 4 wt.% H_2O at pressures of 3–5 kbars. These temperatures are in good agreement with those inferred by Moore and Sisson (2008) for the K-feldspar megacrysts of the Sierra Nevada batholith. These authors, using a Zr-in-titanite geothermometer, calculated a growth temperature range of 735–760°C for titanite crystals included within K-feldspar megacrysts. In addition, the location of the K-feldspar saturation boundary determined experimentally broadly agrees with relations in haplogranitic systems and assemblage stability diagrams (i.e. pseudosections) constructed for the Peninsula

pluton using internally consistent sets of thermodynamic data by Villaros et al. (2009b). Therefore, this combined evidence suggests that the magmatic structures involving K-feldspar megacrysts in the Peninsular Pluton formed by localized magma flow and melt–crystals separation at a temperature not exceeding 750°C in a crystal-rich magma chamber. At this temperature the magma contains about 50 vol.% of crystals, as extrapolated from the pseudosections calculated at 10 kbars by Villaros et al. (2009b). This value matches with experimental evidence indicating that when K-feldspar begins to crystallize in granites, the magma typically contains 60–70 % liquid (Clemens and Wall 1981; Vernon and Paterson 2008).

Connecting magmatic structures with the incremental growth of the pluton

Repeated magma injections allow dramatic fluctuations in melt fraction and may induce magma flow and formation of magmatic structures in two ways. First, replenishment of a crystal-rich magmatic system with a new influx of magma that is compositionally similar, but hotter and less crystalline (therefore less dense and less viscous) than earlier magma batches, generates thermal and compositional anomalies producing density variations that may induce convective currents enhancing melt-crystals separation. In particular, the new magma may form a positively buoyant boundary layer that is gravitationally unstable under the influence of temperature and crystallinity resulting in the development of convective plumes (Weinberg et al. 2001). This behaviour is predicted by the experiments of Jellinek and Kerr (1999) in which convection is triggered by the injection of low density fluids into a more dense fluid. Moreover, convection can be also active within an individual and compositionally homogeneous magma body (i.e. self-mixing) that is heated from below by underplating of hot magma. In this case the new magma that intrudes at the base of the chamber generates a thermally boundary layer in the overlying main magma body that locally becomes unstable giving rise to convective plumes (Couch et al. 2001).

Alternatively, magma flow in the melt-bearing system may be directly caused by injection in a crystal-rich mush of newly arriving magma pulses. In fact, magma batches may intrude as dikes through a partially solidified intrusion that is rigid enough (i.e. low percentage of melt) to fracture at dike-emplacement strain rates. The magmatic structures characterizing the Peninsula pluton may form when the crystal-rich host contains enough melt to allow melt-crystals segregation. The upward propagation of dikes within the intrusion terminates where the dikes encounter a relatively abrupt contrast in strength either with a more rigid (more crystal-rich) overlying zone or with a crystal-poor horizon that is too weak to sustain fracture (Miller et al. 2011).

The high chemical variability exhibited by the monzogranite indicates that the different increments building up the pluton did not mix efficiently. This is not surprising because stirring any compositional heterogeneity by convection in crystal-rich silicic (highly viscous) magmas such as the Peninsula monzogranite, is unavoidably slow and difficult. According to Huber et al. (2009) efficient stirring of new heterogeneities such as those introduced by new injections of magma in the chamber, requires about 5–10 overturns to be homogenized while a single episode of destabilization of a boundary layer leads to no more than one single overturn. Hence, before reaching a stable configuration, convection in highly viscous systems is only able to partially stir the new heterogeneities that it has introduced.

It is noteworthy that the origin of large K-feldspar crystals has been related to the incremental growth model. Moore and Sisson (2008), studying four K-feldspar megacrystic granitic plutons and related dikes in the Sierra Nevada composite batholiths, conclude that K-feldspar megacrysts form by repeated replenishment of the magma bodies by granitic melt. Multiple injections of new magma generate temperature fluctuations just above alkali-feldspar stability for extended time periods and provided the chemical components necessary for the growth of these extraordinarily large K-feldspar phenocrysts. A similar explanation has been proposed by Berger and Roselle (2001) studying the Crystal Size Distribution of K-feldspar megacrysts in migmatite leucosomes. In this case, the temperature of the system is controlled by a feedback mechanism involving the latent heat of crystallization: after a first stage of growth, the heat released during crystallization produces a slight temperature increase able to interrupt nucleation but not crystal growth.

Processes overprinting source-controlled magma chemical variability

The occurrence of the wide range of magmatic structures and enclaves that have been described here for the first time, challenges important aspects of the model proposed by Stevens et al. (2007) and Villaros et al. (2009a, b, 2012), that consider the chemical variability exhibited by the Peninsula pluton to be directly inherited from a heterogeneous metasedimentary source.

In particular, relevant questions are: how and to what extent can the original chemical variability of the system be modified by the late stage magma flow that produced the magmatic structures? Were the magmas which crystallize the microgranitoid and porphyritic granodiorite enclaves produced by melting of the same (or similar) source that generated the Peninsula monzogranite? In a more general

sense, what is the role played by various petrogenetic processes that form the magmatic structures in shaping the compositional diversity of the magma? It is important to mention that in the discussion which follows, unless clearly specified, we refer to the volumetrically dominant Peninsula monzogranite that forms approximately 95 vol.% of the pluton.

Magmatic structures: the role of fractional crystallization

The magmatic structures described for the Peninsula pluton represent evidence that fractional crystallization operated during and/or after pluton emplacement. Here we evaluate how the accumulation of crystals in pipes, mafic mineral aggregates and biotite-rich schlieren influences the composition of the pluton to determine how and to what extent its chemical variability could be related to fractional crystallization by flow segregation.

Pipes are the most common structures in the pluton and although they are locally clustered up to a maximum density of about 5 pipes every 100 m^2, corresponding to a total volume in the granite of 2–3 %, their average modal abundance has been estimated to be less than 1 %. We consider an average pipe consisting of 80 vol.% of K-feldspar megacrysts and for the remaining 20 vol.% of a mineral assemblage representative of the composition of the average granitic host. The resulting composition has been used to evaluate the effect of K-feldspar accumulation into the pipe structures on the major and trace element composition of the pluton. It is noteworthy that the occurrence of pipes does not significantly influence the ferromagnesian content of the system and thus their genesis is unable to explain the broad range in MgO + FeO^T displayed by the Peninsular Pluton. The vector x_1 (Fig. 9) represents the removal of 10 % of pipes from the average granite composition, i.e. an order of magnitude more than the estimated amount of pipe material in the pluton. The resultant vector indicates that the scatter in K_2O content characteristic of the pluton cannot be explained by a simple process of K-feldspar segregation in pipes. Therefore, this process has only a minor influence on the bulk composition of the rock.

Mafic mineral aggregates are rarer than pipes and their modal abundance in the pluton is less than 0.1 %. The abundance of ferromagnesian phases and K-feldspar megacrysts in mafic aggregates is strongly variable, and within individual aggregates different phases tend to form separated domains so that the aggregate average composition is difficult to estimate. However, assuming that ferromagnesian phases form 50 vol.% of mafic aggregates the composition of the magma from which they segregate can be estimated. The genesis of 0.1 vol.% of mafic aggregates accounts for variation in the FeO^T + MgO content of the system of about 0.1 wt.%, more than 40 times lower than the variability exhibited by the Peninsula monzogranite.

Two important lines of evidence argue against fractional crystallization as a likely general process to explain the chemical variability exhibited by the pluton. Firstly, as discussed by Stevens et al. (2007), to explain the more mafic composition of the monzogranite with respect to average experimental melts, a large volume of very silicic compositions would be needed to counterbalance the relatively mafic rocks (i.e. the monzogranite) hypothetically produced by fractional crystallization from experimental-like silicic melts. The required large volumes of highly silicic rocks are absent from the preserved rock record. Secondly, the tight positive correlation between TiO_2 and MgO + FeO^T cannot be produced by fractionation of biotite, the only rock-forming phase containing significant amounts of TiO_2, MgO, FeO^T, as biotite fractionation would also generate positive correlations between K_2O and MgO + FeO^T (Fig. 9, vectors x_2) and between K_2O and TiO_2. These are not observed.

Fractional crystallization appears to have a significant role in shaping the chemical composition of coarse-grained mafic enclaves. In fact, although these enclaves represent the most ferromagnesian rocks in the pluton, they are characterized by Nd isotope composition identical to that of the monzogranite suggesting that the two rock types formed by partial melting of the same source. The origin of coarse-grained mafic enclaves may be explained in two ways. Firstly, they may have formed by fractionation of about 5–10 wt.% of plagioclase from a magma that entrained about 30–35 wt.% of peritectic garnet and ilmenite. This hypothesis fits with the enclaves plotting on the MgO + FeO^T vs. TiO_2 trend generated by samples from the Peninsula monzogranite (Fig. 9) as well as with their well-defined negative correlation for MgO + FeO^T vs. CaO, Na_2O, Ba and Sr and their pronounced negative Eu anomaly. An alternative explanation is that coarse-grained mafic enclaves represent autolith formed by accumulation of garnet and orthopyroxene crystals in a plagioclase-bearing magmatic system. The enclaves are remobilized and dispersed within the magma chamber by the emplacement of subsequent magma batches. This model is consistent with the high petrographic and chemical variability characteristic of this enclave-type as well as with their characteristic coarse-grained texture.

Microgranitoid and granodioritic enclaves: mixing with a primitive magma

Calc-alkaline granitoids commonly host fine- to medium-grained, distinctively dark-coloured magmatic enclaves (often called “mafic microgranular enclaves”) that are commonly interpreted as globules of more mafic magma which mingled with and chilled against the cooler, more felsic host magma (e.g. Vernon 1990; Barbarin 2005). We explain

microgranitoid and porphyritic granodiorite enclaves in the Peninsula pluton as formed by chemical and physical interaction between a calc-alkaline peraluminous magma having a composition similar to the Peninsula monzogranite and a low-K, more mafic component whose initial composition is never preserved in the rock record. Two lines of evidence favour this interpretation. Firstly, although the initial Nd-isotope ratios for the different rocks largely overlap, both enclave-types appear to have higher εNd than the Peninsula monzogranite. Microgranitoid enclaves have the highest εNd recorded in the whole system while εNd values for porphyritic enclaves are intermediate between those of the microgranitoid enclaves and those of the Peninsula monzogranite (Fig. 11). The more juvenile isotopic composition of the enclaves argues against a co-magmatic origin for these enclaves and their host, suggesting derivation of the enclaves from a different source. Secondly, large K-feldspar, plagioclase and cordierite crystals from the monzogranite have been partly or completely physically incorporated into the enclaves (Fig. 5d, f) supporting crystal transfer as a hybridization mechanism. In microgranitoid enclaves, megacrysts commonly straddle the host-enclave boundary and have textural and compositional features identical to megacrysts in the host. On the other hand, K-feldspar megacrysts in granodioritic enclaves, although texturally and compositionally similar to those in the host monzogranite, show evidences of chemical interaction with the surrounding enclaves. In particular, they have rounded morphology and size that is slightly to substantially smaller than those characteristic of megacrysts in the host.

Microgranular enclaves have higher MgO and FeO^T and lower K_2O than granodioritic enclaves and thus their compositions can be used to speculate on the nature of the more mafic magma involved. They have a K_2O content (≈2.5 wt.%) that is significantly lower than that for experimental melts obtained by biotite fluid-absent melting of mature sources (i.e. metagreywacke and metapelites) as well as by melting of moderately hydrous (1.7–2.3 wt.% H_2O) medium-to-high K basaltic compositions (Sisson et al. 2005). Moreover, microgranitoid enclaves have a relatively primitive εNd and host biotites that are markedly more MgO-rich than those in the Peninsula pluton. These data suggest that microgranular enclaves were derived by amphibole fluid absent melting of immature sediments or by partial melting of tholeiitic basalts. It is worth noting that mafic and intermediate intrusions in the Cape Granite Suite are volumetrically insignificant, substantially younger (i.e. 519±7 Ma) than the pluton and mostly too rich in K_2O to be a suitable mafic end-member (Joordan et al. 1995).

A further important question is to what extent interaction with the mafic end-member magma has modified the composition of the volumetrically predominant peraluminous magma. Mixing with a microgranitoid enclave-like end-member cannot consistently explain the major and trace element composition of the Peninsula monzogranite. In particular, microgranitoid enclaves do not plot on many of the linear arrays described. They have higher SiO_2 and lower Y, Nb, Th and Zr than expected from their MgO + FeO^T composition and, in spite of the almost identical MgO + FeO^T composition of the different samples, they display variable TiO_2 contents. This has been identified as a feature to be expected of hybrid magmas arising by interaction between basalts and granites, where the variable TiO_2 vs. MgO + FeO^T that is inherent to basaltic magmas disturbs the tight correlation that is inherent to granites through the peritectic assemblage entrainment process (Clemens et al. 2011). In addition, microgranitoid and porphyritic granodiorite enclaves in the pluton are scarce compared to other S-type granites (e.g. Deddick Granodiorite; Maas et al. 1997) and coeval mafic dikes are lacking suggesting limited influence of more mafic magmas in determining the composition of the host granite.

The occurrence of K-feldspar megacrysts in the enclaves indicates that hybridization through crystal transfer continued at depth down to the temperature of alkali feldspar crystallization in the peraluminous magma (i.e. 770–750° C). Blobs of more mafic magmas were transported to the emplacement level where, due to their higher solidus temperature they experienced a higher degree of undercooling resulting in their typical fine to medium grained groundmass. The more mafic, denser magma did not efficiently mix with the previously emplaced more silicic magma. However, as described by Couch et al. (2001) the "underplating" of hotter magma is potentially able to heat the silicic magma chamber forming layers of hot silicic magma at depth that becomes buoyant and unstable resulting in the development of convective plumes.

Conclusions

A complex array of widespread magmatic structures and enclaves is preserved in the Peninsula pluton. The ubiquitous involvement of large K-feldspar crystals in the magmatic structures suggests that they form by localized magma flow in crystal-rich mushes (i.e. ≈50 vol.% crystals) at about 750° C. The energy required to trigger and sustain flow in the high viscosity magmatic system is supplied by injection of magma batches in two ways: the new magma intrudes the base of the magma reservoir and forms a positively buoyant boundary layer that is gravitationally instable because hotter and less crystalline (therefore less dense and less viscous) than the surroundings, and/or magma increments intrudes within the partially crystallized magma chamber. Repeated replenishments of the magmatic system generate the waxing and waning of the temperature field and allow fluctuations in melt fraction and volume of mobile magma within the pluton. This

process can be responsible for the peculiar growth to nucleation rate conditions that allow the formation of K-feldspar megacrysts as argued by Moore and Sisson (2008).

The large chemical variability exhibited by the monzogranite proves that the different batches were unable to homogenize as also attested by the occurrence of magmatic structures representing "snapshots" of the stirring process. The batches inherited their composition directly from the source as described by Stevens et al. (2007) and Villaros et al. (2009a, b, 2012) while the role of processes such as fractional crystallization and mixing with more juvenile magmas is marginal and limited to the genesis of magmatic structures and enclaves. In the Peninsula pluton, the incremental emplacement of discrete magma pulses leads to the development of internal variations in temperature and therefore viscosity and buoyancy leading to internal stirring originating a number of magmatic structures.

Acknowledgments The authors gratefully acknowledge support from the NRF through SARChI funding to GS. We thank Chris Harris and Roberto Weinberg for their critical and constructive comments which helped us to improve significantly the original manuscript.

References

Annen C (2011) Implications of incremental emplacement of magma bodies for magma differentiation, thermal aureole dimensions and plutonism-volcanism relationships. Tectonophysics 500:3–10

Bachmann O, Bergantz GW (2008) Rhyolites and their source mushes across tectonic settings. J Petrol 49(12):2277–2285

Barbarin B (2005) Mafic magmatic enclaves and mafic rocks associated with some granitoids of the central Sierra Nevada batholith, California: nature, origin, and relations with the hosts. Lithos 80:155–177

Barrière M (1981) On curved laminae, graded layers, convection currents and dynamic crystal sorting in the Ploumanac'h (Brittany) subalkaline granite. Contrib Mineral Petrol 77:214–224

Belcher RW, Kisters AFM (2003) Lithostratigraphic correlations in the western branch of the Pan-African Saldania Belt, South Africa: the Malmesbury Group revisited. S Afr J Geol 106:327–342

Berger A, Roselle G (2001) Crystallization process in migmatites. Am Mineral 86(3):215–224

Clarke DB, Clarke GKC (1998) Layered granodiorites at Chebutco Head, South Mountain batholith, Nova Scotia. J Struct Geol 20:1305–1324

Clemens JD, Wall JV (1981) Origin and crystallization of some peraluminous (S-type) granitic magmas. Can Mineral 19:111–131

Clemens JD, Wall VJ (1984) Origin and evolution of a peraluminous silicic ignimbrite suite: the Violet Town Volcanics. Contrib Mineral Petrol 88:354–371

Clemens JD, Helps PA, Stevens G (2009) Chemical structure in granitic magmas—a signal from the source? Trans R Soc Edinb Earth Sci 100:1–14

Clemens JD, Benn K (2010) Anatomy, emplacement and evolution of a shallow-level, post-tectonic laccolith: the Mt Disappointment pluton, SE Australia. J Geol Soc 167:915–941

Clemens JD, Stevens G, Farina F (2011) The enigmatic sources of I-type granites: the peritectic connexion. Lithos 126:174–181. doi:10.1016/j.lithos.2011.07.004

Clemens JD, Stevens G (2012) What controls chemical variation in granitic magmas? Lithos 134–135:317–329

Coleman DS, Gray W, Glazner AF (2004) Rethinking the emplacement and evolution of zoned plutons: geochronologic evidence for incremental assembly of the Tuolumne Intrusive Suite, California. Geology 32:433–436

Couch S, Sparks RSJ, Carroll MR (2001) Mineral disequilibrium in lavas explained by convective self-mixing in open magma chambers. Nature 411:1037–1039

Darwin CR (1844) Geological observations on the volcanic islands visited during the voyage of H.M.S. Beagle, together with some brief notices of the geology of Australia and the Cape of Good Hope. Being the second part of the geology of the voyage of the Beagle, under the command of Capt. Fitzroy, R.N. during the years 1832 to 1836. Smith Elder and Co, London

Da Silva L, Gresse P, Scheepers R, McNaughton NJ, Hartmann LA, Fletcher I (2000) U-Pb SHRIMP and Sm-Nd age constraints on the timing and sources of the Pan-African Cape Granite Suite, South Africa. J Afr Earth Sci 30:795–815

Davidson JP, Morgan DJ, Charlier BLA, Harlou R, Hora JM (2007) Microsampling and isotopic analysis of igneous rocks: implications for the study of magmatic systems. Annu Rev Earth Planet Sci 35:273–311

Eggins S (2003) Laser ablation ICP-MS analysis of geological materials prepared as lithium borate glasses. Geostand Geoanal Res 27:147–162

Farina F, Dini A, Innocenti F, Rocchi S, Westerman DS (2010) Rapid incremental assembly of the Monte Capanne pluton (Elba Island, Tuscany) by downward stacking of magma sheets. Geol Soc Am Bull 122(9–10):1463–1479

Gardien V, Thompson AB, Grujic D, Ulmer P (1995) Experimental melting of biotite + plagioclase + quartz ± muscovite assemblages and implications for crustal melting. J Geophys Res 100 (B8):15581–15591

Glazner AF, Bartley JM, Coleman DS, Gray W, Taylor RZ (2004) Are plutons assembled over millions of years by amalgamation from small magma chambers? GSA Today 14:4–11

Gresse PG, Scheepers R (1993) Neoproterozoic to Cambrian (Namibian) rocks of South Africa: a geochronological and geotectonic review. J Afr Earth Sci 16:375–393

Harris C, Faure K, Diamond RE, Scheepers R (1997) Oxygen and hydrogen isotope geochemistry of S- and I-type granitoids: the Cape Granite suite, South Africa. Chem Geol 143:95–114

Harris C, Vogeli J (2010) Oxygen isotope composition of garnet in the Peninsula granite, Cape Granite Suite, South Africa: constraints on melting and emplacement mechanisms. S Afr J Geol 113(4):385–396

Hasalová P, Weinberg RF, Macrae C (2011) Microstructural evidence for magma confluence and reusage of magma pathways: implications for magma hybridization, Karakoram Shear Zone in NW India. J Metamorph Geol 29:875–900

Holdaway MJ (2000) Application of new experimental and garnet Margules data to the garnet–biotite geothermometer. Am Mineral 85:881–892

Huber C, Bachmann O, Manga M (2009) Homogenization processes in silicic magma chambers by stirring and mushification (latent heat buffering). Earth Planet Sci Lett 283:38–47

Jellinek AM, Kerr RC (1999) Mixing and compositional stratification produced by natural convection: 2. Applications to the differentiation of basaltic and silicic magma chambers and komatiite lava flows. J Geophys Res 104:7203–7218

Joordan LJ, Scheepers R, Barton ES (1995) Geochemistry and isotopic composition of the mafic and intermediate igneous components of the Cape Granite Suite, South Africa. J Afr Earth Sci 21:59–70

Johnson BR, Glazner AF (2009) Formation of K-feldspar megacrysts in granodioritic plutons by thermal cycling and late-stage textural coarsening. Contrib Mineral Petrol 159(5):599–619

Maas R, Nicholls IA, Legg C (1997) Igneous and metamorphic enclaves in the S-type Deddick Granodiorite, Lachlan Fold Belt, SE Australia: petrographic, geochemical and Nd–Sr isotopic evidence for crustal melting and magma mixing. J Petrol 38(7):815–841

Matzel JP, Bowring SA, Miller RB (2006) Time scales of pluton construction at different crustal levels; examples from the Mount Stuart and Tenpeak intrusions, North Cascades, Washington. Geol Soc Am Bull 118:1412–1430

Michel J, Baumgartner L, Putlitz B, Schaltegger U, Ovtcharova M (2008) Incremental growth of the Patagonian Torres del Paine laccolith over 90 k.y. Geology 36(6):459–462

Míková J, Denková P (2007) Modified chromatographic separation scheme for Sr and Nd isotope analysis in geological silicate samples. J Geosci 52:221–226

Miller CF, Furbish DJ, Walker BA, Claiborne LL, Koteas GC, Bleick HA, Miller JS (2011) Growth of plutons by incremental emplacement of sheets in crystal-rich host: evidence from Miocene intrusions of the Colorado River region, Nevada, USA. Tectonophysics 500:65–77

Montel JM, Vielzeuf D (1997) Partial melting of metagreywackes, part II. Compositions of minerals and melts. Contrib Mineral Petrol 128:176–196

Moore JG, Sisson TW (2008) Igneous phenocrystic origin of K-feldspar megacrysts in granitic rocks from the Sierra Nevada batholith. Geosphere 4(2):387–400

Moyen JF, Stevens G, Kisters A (2006) Record of mid-Archaean subduction from metamorphism in the Barberton terrain, South Africa. Nature 442:559–562

Paterson SR, Vernon RH, Žák J (2005) Mechanical instabilities and physical accumulation of K-feldspar megacrysts in granitic magma, Tuolumne Batholith, California, USA: J Virtual Explorer, ISSN 1441-8142, 18, 1

Paterson SR (2009) Magmatic tubes, pipes, troughs, diapirs, and plumes: late-stage convective instabilities resulting in compositional diversity and permeable networks in crystal-rich magmas of the Tuolumne batholith, Sierra Nevada, California. Geosphere 5:496–527

Patiño Douce AE, Johnston AD (1991) Phase equilibria and melt productivity in the pelitic system: implications for the origin of peraluminous granitoids and aluminous granulites. Contrib Mineral Petrol 107:202–218

Patiño Douce AE, Beard JS (1996) Effect of P, $f(O_2)$ and Mg/Fe ratio on dehydration melting of model metagreywackes. J Petrol 37 (5):999–1024

Patiño Douce AE, Harris N (1998) Experimental constraints on Himalayan anatexis. J Petrol 39(4):689–710

Pearce NJG, Perkins WT, Westgate JA, Gorton MP, Jackson SE, Meal CR, Chenery SP (1997) A compilation of new and published major and trace element data for NIST SRM 610 and NIST SRM 612 glass reference materials. Geostand Newslett 21:115–144

Pickering JM, Johnston DA (1998) Fluid-absent melting behaviour of a two mica metapelite: experimental constraints on the origin of Black Hill Granite. J Petrol 39(10):1787–1804

Piwinskii AJ (1968) Experimental studies of igneous rock series, central Sierra Nevada Batholith, California. J Geol 76:548–570

Reichardt H, Weinberg RF, Andersson UB, Fanning CM (2010) Hybridization of granitic magmas in the source: the origin of the Karakoram Batholith, Ladakh, NW India. Lithos 116:249–272

Rozendaal A, Gresse PG, Scheepers R, LeRoux JP (1999) Neoproterozoic to early Cambrian crustal evolution of the Pan-African Saldania Belt, South Africa. Precambrian Res 97:303–323

Sawyer EW (1996) Melt segregation and magma flow in migmatites: implications for the generation of granite magmas. Trans R Soc Edinb Earth Sci 87:85–94

Scheepers R (1995) Geology, geochemistry and petrogenesis of late Precambrian S-, I and A-type granitoids in the Saldania Belt, Western Cape Province, South Africa. J Afr Earth Sci 21:35–58

Scheepers R, Armstrong RA (2002) New U-Pb SHRIMP zircon ages of the Cape Granite Suite: implications for the magmatic evolution of the Saldania Belt. S Afr J Geol 105:241–256

Scheepers R, Poujol M (2002) U-Pb zircon age of Cape Granite Suite ignimbrites: characteristics of the last phases of the Saldaniaan Magmatism. S Afr J Geol 105:163–178

Sisson TW, Ratajeski K, Hankins WB, Glazner AF (2005) Voluminous granitic magmas from common basaltic sources. Contrib Mineral Petrol 148:635–661

Stevens G, Clemens JD, Droop GTR (1997) Melt production during granulite-facies anatexis: experimental data from "primitive" metasedimentary protoliths. Contrib Mineral Petrol 128:352–370

Stevens G, Villaros A, Moyen JF (2007) Selective peritectic garnet entrainment as the origin of geochemical diversity in S-type granites. Geology 35(1):9–12

Tanaka T, Togashi S, Kamioka H, Amakawa H, Kagami H, Hamamoto T, Yuhara M, Orihashi Y, Yoneda S, Shimizu H, Kunimaru T, Takahashi K, Yanagi T, Nakano T, Fujimaki H, Shinjo R, Asahara Y, Tanimizu M, Dragusanu C (2000) JNdi-1: a neodymium isotopic reference in consistency with LaJolla neodymium. Chem Geol 168:279–281

Vernon RH (1990) Crystallization and hybridism in microgranitoid enclave magmas: microstructural evidence. In: Sawka WN, Hildebrand RS (eds) Mafic inclusion in granites. J Geophys Res 95: 17849–17859

Vernon RH, Paterson SR (2008) How late are K-feldspar megacrysts in granites? Lithos 104:327–336

Vernon RH (2010) Granites really are magmatic: using microstructural evidence to refute some obstinate hypotheses. In: Forster MA, Fitz Gerald JD (eds) Journal of the Virtual Explorer 35: 1, doi:10.3809/jvirtex.2011.00264

Vielzeuf D, Holloway JR (1988) Experimental determination of the fluid-absent melting relations in the pelitic system. Consequences for crustal differentiation. Contrib Mineral Petrol 98:257–276

Vielzeuf D, Montel JM (1994) Partial melting of metagreywackes. Part I. Fluid-absent experiments and phase relationships. Contrib Mineral Petrol 117:375–393

Villaros A, Stevens G, Moyen JF, Buick IS (2009a) The trace element composition of S-type granites: evidence for disequilibrium melting and accessory phase entrainment in the source. Contrib Mineral Petrol 158:543–561

Villaros A, Stevens G, Buick IS (2009b) Tracking S-type granite from source to emplacement: clues from garnet in the Cape Granite Suite. Lithos 112(3–4):217–235

Villaros A, Buick IS, Stevens G (2012) Isotopic variations in S-type granites: an inheritance from a heterogeneous source. Contrib Mineral Petrol 163:243–257. doi:10.1007/s00410-011-0673-9

Weinberg RF, Sial AN, Pessoa R (2001) Magma flow within the Tavares pluton, northeastern Brazil: compositional and thermal convection. Geol Soc Am Bull 113:508–520

Weis D, Kieffer B, Maerschalk C, Barling J, de Jong J, Williams GA, Hanano D, Pretorius W, Mattielli N, Scoates JS, Goolaerts A, Friedman RM, Mahoney GB (2006) High-precision isotopic characterization of USGS reference materials by TIMS and MC-ICP-MS. G^3 7, Q08006, doi:10.1029/2006GC001283

Wiebe RA, Jellinek M, Markley MJ, Hawkins DP, Snyder D (2007) Steep schlieren and associated enclaves in the Vinalhaven granite, Maine: possible indicators for granite rheology. Contrib Mineral Petrol 153:121–138

Žák J, Klomínsky J (2007) Magmatic structures in the Krkonoše-Jizera plutonic complex, Bohemian Massif: evidences for localized multiphase flow and small scale thermal-mechanical instabilities in a granitic magma chamber. J Volcanol Geotherm Res 164:254–267